Comparing Sampling Efficiency in Particulate Materials Using Characteristic Functions: An Empirical Study of Scoop vs Riffle Methods

By Richard Minnitt[1]

DOI: 10.62178/sst.005.002

ABSTRACT

Representative sampling of particulate materials remains a critical challenge across scientific and industrial domains, yet traditional method comparisons based on means and variances fail to capture complete distributional differences. This study introduces Characteristic Function (CF) analysis as a comprehensive statistical framework for evaluating sampling methods, providing a complete spectral representation of sampling distributions that reveals features hidden from conventional statistics. We empirically compared two common methods, scoop sampling and riffle splitting, using four density tracers (blue corn at 1.3 g/cm^3, steel at 7.8 g/cm^3, lead at 11.3 g/cm^3, and tungsten carbide at 14.9 g/cm^3) mixed in a popcorn matrix, with 32 samples per method analysed for both particle counts and individual mass measurements. Results demonstrate that while both methods captured similar mean counts, riffle splitting maintained near-ideal Poisson behaviour across all density ranges (variance-to-mean ratio = 0.77–0.93), whereas scoop sampling exhibited severe density-dependent over-dispersion (variance-to-mean ratio up to 19.33) and failed to capture heavy particles in 28 – 47 % of samples. CF analysis revealed fundamental distributional differences (integrated CF distance D = 0.324), with scoop sampling producing multimodal, heavy-tailed distributions with oscillatory CF signatures indicative of particle clumping, while riffle splitting generated smooth, unimodal distributions approaching Gaussian form. The riffle method demonstrated superior performance across all metrics: perfect detection sensitivity, statistical independence between tracer captures (factorization error 4.9× lower), consistent mass measurements (CV 3.7–6.1× lower), and strong count-mass linearity ($r > 0.98$). A composite scoring system integrating six performance dimensions ranked riffle splitting significantly higher (0.89/1.00) than scoop sampling (0.60/1.00). This study establishes Characteristic Function analysis as a powerful diagnostic tool that bridges theoretical sampling science and practical method validation, providing evidence-based recommendations for particulate sampling protocols and a generalizable template for evaluating any sampling method applied to heterogeneous materials.

1. Introduction

1.1 The Sampling Problem in Particulate Materials

Representative sampling of particulate materials stands as a critical yet persistently challenging task across numerous industrial and scientific domains. From mineral processing and pharmaceutical manufacturing to food production and environmental monitoring, the ability to obtain samples that accurately reflect the composition of bulk materials directly impacts product quality, process efficiency, and economic outcomes [1,2].

Despite decades of research and standardization efforts, sampling remains what Pierre Gy famously termed "the Achilles' heel" of analytical chemistry [3], with sampling errors often exceeding analytical errors by orders of magnitude.

The fundamental challenge arises from the heterogeneous nature of particulate materials, where components of interest—whether mineral grains, agricultural grains, active pharmaceutical ingredients, or contaminants—are rarely distributed uniformly throughout the bulk.

1 School of Mining Engineering, University of the Witwatersrand, Johannesburg, South Africa

This heterogeneity manifests at multiple scales: microscopic variations in individual particle composition, mesoscopic clustering or segregation patterns, and macroscopic distribution gradients [3,4]. When sampling such materials, every extraction act introduces bias, the magnitude of which depends not only on the sampling method itself but also on the material's inherent heterogeneity and the sampler's interaction with it.

Traditional approaches to evaluating sampling methods have largely relied on comparative statistics—comparing means, variances, or conducting t-tests between methods [4,5,9]. While these methods provide some insight, they suffer from a critical limitation: they reduce complex, multidimensional distributional information to a few summary statistics. This is akin to describing a symphony by reporting only its average volume and duration while ignoring melody, harmony, and rhythm. Two sampling methods might produce identical mean compositions while capturing fundamentally different distributions, with one method systematically oversampling clusters while another provides truly representative samples.

1.2 The Characteristic Function: A Statistical "X-ray" for Distribution Analysis

The Characteristic Function (CF) is a powerful yet underutilized tool in the sampling scientist's arsenal. First introduced as an analytical method by Lagrange around 1770, the first general definition of the characteristic function is attributed to Laplace in his 1812 work, *Théorie analytique des probabilités* [7]. In this work, Laplace effectively used what we now recognize as the Fourier transform—an integral transform rooted in his own earlier probability studies from the 1780s, as a tool for probabilistic analysis. While Fourier's 1822 treatise later formalized the transform that bears his name [8], the underlying mathematical ideas were already present in Laplace's work.

The CF as we know it today was formalized in the early 20th century, primarily through the work of Paul Lévy and Aleksandr Khinchin. Lévy's 1937 monograph, *Théorie de l'addition des variables aléatoires* [9], established the fundamental properties of characteristic functions and used them to prove general versions of the Central Limit Theorem. Independently, Khinchin made parallel contributions to the theory of limit theorems and stationary processes [7,9]. Through their efforts, the characteristic function became a complete description of a probability distribution through its Fourier transform. Mathematically defined as $\varphi_X(t) = E[e^{\{itX\}}]$, where i is the imaginary unit and $t \in R$ is a real-valued parameter, the CF encodes all information about the distribution of the random variable X.

What makes the CF particularly valuable for sampling analysis is its dual nature as both a comprehensive descriptor and a practical computational tool. Unlike probability density functions that can be difficult to estimate and compare, CFs offer several advantages for sampling studies:

a) **Completeness**: The CF uniquely determines the distribution, so no information is lost in the transformation.
b) **Additivity**: For independent random variables, the CF of their sum equals the product of their individual CFs, making it ideal for analysing particle counts.
c) **Moment generation**: All moments of the distribution can be recovered through differentiation at the origin: $E[X^k] = (-i)^k \varphi_X^k(0)$, where $\varphi_X^k(0)$ denotes the k-th derivative of the characteristic function evaluated at $t = 0$.
d) **Numerical stability**: CFs are often better behaved than density functions for empirical estimation, requiring no tuning parameters like bandwidths.

In the context of particulate sampling, CFs serve as a kind of "statistical X-ray," revealing the internal structure of sampling distributions that remain hidden to conventional analysis. They allow us to answer fundamental questions like: Do two sampling methods produce the same underlying distribution? Are different particle types sampled independently? How does sample mass affect distribution shape?

The relevance of CFs to particulate sampling was established by Venter [5], who modelled trace analyte concentrations using compound Poisson distributions derived from CFs, elegantly establishing the connection to particulate sampling, a topic covered in some detail by Lyman [6,7]. However, the application of CFs to compare different physical sampling methods, particularly for multi-tracer systems with both count and mass data, remains largely unexplored. This study addresses that gap.

1.3 Research Objectives and Study Design

This study addresses this gap by applying Characteristic Function analysis to compare two common sampling methods: scooping and riffle splitting for particulate materials.

Our investigation has four primary objectives:

a) **Pedagogical**: To explain Characteristic Functions in accessible terms, demonstrating their utility beyond theoretical statistics.
b) **Methodological**: To develop a comprehensive CF-based framework for sampling method comparison.
c) **Empirical**: To apply this framework to experimental data from four density tracers, analysing both particle counts and mass distributions.
d) **Practical**: To provide evidence-based recommendations for sampling practitioners and quality control systems.

An experimental study was conducted using four distinct density tracers, blue corn (lightest), steel balls, lead balls, and tungsten carbide (heaviest), mixed in a controlled particulate matrix of popcorn maize. Thirty-two samples were collected using each method, with both particle counts and individual mass measurements recorded. This design allows us to examine not only how many particles of each type are captured, but also whether the captured particles are representative in terms of size/mass distribution. The analysis proceeds through traditional descriptive statistics that provide a baseline comparison, followed by CF analysis which reveals underlying characteristics of the distributions. The independence between tracers is examined together with the consistency of mass measurements, addressing the fundamental question: "Which method produces samples that better represent the true composition of the material?" This research aims to demonstrate that Characteristic Functions capture the full complexity of particulate heterogeneity and offer a more nuanced and informative approach to sampling method evaluation, while providing actionable insights for practical sampling applications.

Introductory figures (Figs. 1–3) are theoretical and use simulated data to introduce the characteristic function (CF) concept and typical spectral signatures of distributions relevant to particulate sampling, using purely simulated data; no experimental data are used in Figs. 1–3. Experimental results (Figs. 4–7 and Tables 4–12), drawn from the study data in SR.xlsx, demonstrate CF analysis in practice and enable a practical comparison of sampling methods. Both components are essential: the theory builds understanding of CFs, while the experiments demonstrate CFs' diagnostic power in real-world sampling.

2. Theoretical Framework of Characteristic Functions

2.1 Definition and Interpretation of the Characteristic Function

Although the characteristic function may initially appear as an abstract construct with little apparent connection to practical sampling, it actually offers a compact, intuitive, and powerful way to characterise randomness by providing a complete spectral representation of its probability distribution. For a real-valued random variable X, the characteristic function (CF) provides a complete representation that uniquely determines its probability distribution and is defined as:

$$\varphi_X(t) = E[e^{itX}] = E[\cos(tX) + i\sin(tX)] \quad (1)$$

Where $i = \sqrt{-1}$ is the imaginary unit, and t ∈ R is a frequency parameter. For a continuous random variable with probability density function $fX(x)$, this becomes the integral:

$$\varphi_X(t) = \int_{-\infty}^{\infty} exp^{itx} f_X(x)dx \quad (2)$$

While for a discrete random variable taking values x_k with probabilities p_k:

$$\varphi_X(t) = \int_{-\infty}^{\infty} exp^{it x_k} p_k \quad (3)$$

There are several interconnected interpretations that clarify the usefulness of Eq. (1).

First, from a probabilistic standpoint, for a random variable *X* (say, the number of tungsten particles in a sample), and for any fixed real number *t*, we compute:

$$\varphi_X(t) = E[e^{itX}] = E[\cos(t_X) + i\sin(t_X)] \quad (4)$$

a point on the complex unit circle whose angle depends on *X*. The Characteristic Function $\varphi(t)$ is simply the average position of this point over many realizations of *X*. If *t* is small, the phase t_X changes slowly with *X*, giving an average near 1+0*i*. If t is large, the angle varies rapidly, and the average tends toward 0+0*i*.

Second, from a transformation perspective: The CF is precisely the Fourier transform of the probability density function $f_x(x)$. Just as a prism separates white light into its constituent colours, the Fourier transform decomposes a probability distribution into its frequency components.

The parameter t represents frequency in this analogy, small t probes large-scale distribution features (like the mean), while large t reveals fine details (like the behaviour in the tails).

Third, and most powerful for comparing the distributions is the generative perspective: The CF contains the complete "DNA" of a probability distribution. Given $\varphi(t)$, one can recover not only the mean and variance but every moment, every quantile, indeed the entire distribution itself through the inverse Fourier transform:

$$f_X(x) = \frac{1}{2\pi}\int_{-\infty}^{\infty} e^{-itx}\varphi_X(t)dt \tag{5}$$

This completeness property makes CFs uniquely suited for comparing distributions, two methods produce identical sampling results if and only if their CFs are identical for all t. Consequently, two sampling methods yield statistically identical results if and only if their characteristic functions are equal for all t. This completeness property is the foundation for using CFs as a rigorous tool for comparing empirical distributions.

2.2 Essential Mathematical Properties

Several mathematical properties make CFs particularly valuable for sampling analysis:

a) Linearity of Expectation:

$$\varphi_{aX+b}(t) = e^{-itb}\varphi_X(at) \tag{6}$$

b) Independence and Convolution: If X and Y are independent:

$$\varphi_{X+Y}(t) = \varphi_X(t)\cdot\varphi_Y(t) \tag{7}$$

c) Moment Generation: The k-th moment exists if $\varphi_X^{(k)}(0)$ exists:

$$E[X^k] = (-i)^k \frac{d^k}{dt^k}\varphi_X(t)\Big|_{t=0} \tag{8}$$

2.3 The Musical Score Analogy: Why Characteristic Functions Work

Consider a musical performance of Beethoven's Fifth Symphony. The actual sound, the waveform measured by a microphone, is analogous to a set of sample measurements: complex, detailed, and unique to each performance. The musical score, by contrast, is a compact representation containing all essential information: notes, rhythms, dynamics, and tempo markings. From the score, one can reconstruct performances (though interpretation introduces variation), compare different orchestras' interpretations, and analyse musical structure.

Characteristic Functions play exactly this role for probability distributions. The probability density function (PDF) is like the audio recording—complete but unwieldy for comparison. The CF is like the musical score—compact yet informationally complete. Just as a musician can compare two performances by examining their scores, we can compare two sampling methods by examining their CFs.

This analogy can be extended to explain several key operations within the characteristic function framework. Each orchestral manipulation has a direct mathematical counterpart in the manipulation of distributions. For instance, a transposition of the composition—shifting all notes to a new key—corresponds to scaling the random variable X by a constant a, as captured by the relation $\varphi aX(t) = \varphi X(at)$. Similarly, the addition of instrumental parts, enriching the overall harmony, is analogous to the convolution of independent random variables. This is mathematically manifested in the multiplicative property of their characteristic functions: for independent X and Y, $\varphi X+Y(t) = \varphi X(t)\cdot\varphi Y(t)$. Harmonic analysis of the score, extracting fundamental frequencies and relationships, parallels the derivation of moments via differentiation of the characteristic function at the origin, where $\varphi(k)(0) = i^k E[X^k]$. Finally, simplification to a piano reduction, which preserves the essential melodic and harmonic structure while omitting full orchestral detail, corresponds to the extraction of marginal distributions from a joint characteristic function by evaluating it with arguments for specific dimensions set to zero.

2.4 Visualizing Characteristic Functions: From Theory to Intuition

Diagrammatic representations shown in Fig. 1 and Fig. 2 present CFs for three distributions relevant to particulate sampling: the Poisson (modelling particle counts), the Normal (approximation for large samples), and a compound Poisson (mixing particle size variations).

Top row of Figure 1 shows probability distributions: (a) Poisson probability mass function ($\lambda = 3$) representing discrete particle counts; (b) Normal probability density function ($\mu = 3$, $\sigma = 1$) representing the large-sample approximation for continuous measurements; (c) Histogram of simulated compound Poisson distribution ($\lambda = 3$, with exponential particle masses of mean 1) representing aggregated particle mass in samples. Bottom row shows the corresponding characteristic functions: (d) Poisson CF exhibiting oscillatory decay, reflecting its discrete nature. The oscillatory pattern in the Poisson CF has fundamental period 2π, reflecting the discrete nature of the distribution. This periodicity is partially visible within the plotted range $t \in [-4, +4]$. (e) Normal CF showing smooth Gaussian decay, characteristic of continuous, well-behaved sampling distributions typical of large sample sizes.

(f) Compound Poisson CF demonstrating intermediate behaviour with heavier tails, characteristic of particulate systems where both particle count and mass vary. All CFs satisfy $\varphi(0) = 1$ (yellow dot), reflecting probability conservation. The magnitude (black dotted line) illustrates decay rates: fastest for Normal (most concentrated), intermediate for Compound Poisson, and slowest with zero-crossings for Poisson (discrete + variable). These spectral signatures provide a complete distributional fingerprint for comparing sampling methods.

Several key features emerge:

a) The unity property: All CFs pass through $\varphi(0) = 1+0i$, reflecting the fact that probabilities sum to one. This serves as a natural "home base" for comparing CFs.
b) The envelope of decay: The magnitude $|\varphi(t)|$ decays with $|t|$, with faster decay indicating "smoother" distributions (more concentrated, fewer extremes). The Poisson CF shows oscillatory decay, revealing its discrete nature.

Figure 5: Characteristic Functions of Distributions Relevant to Particulate Sampling

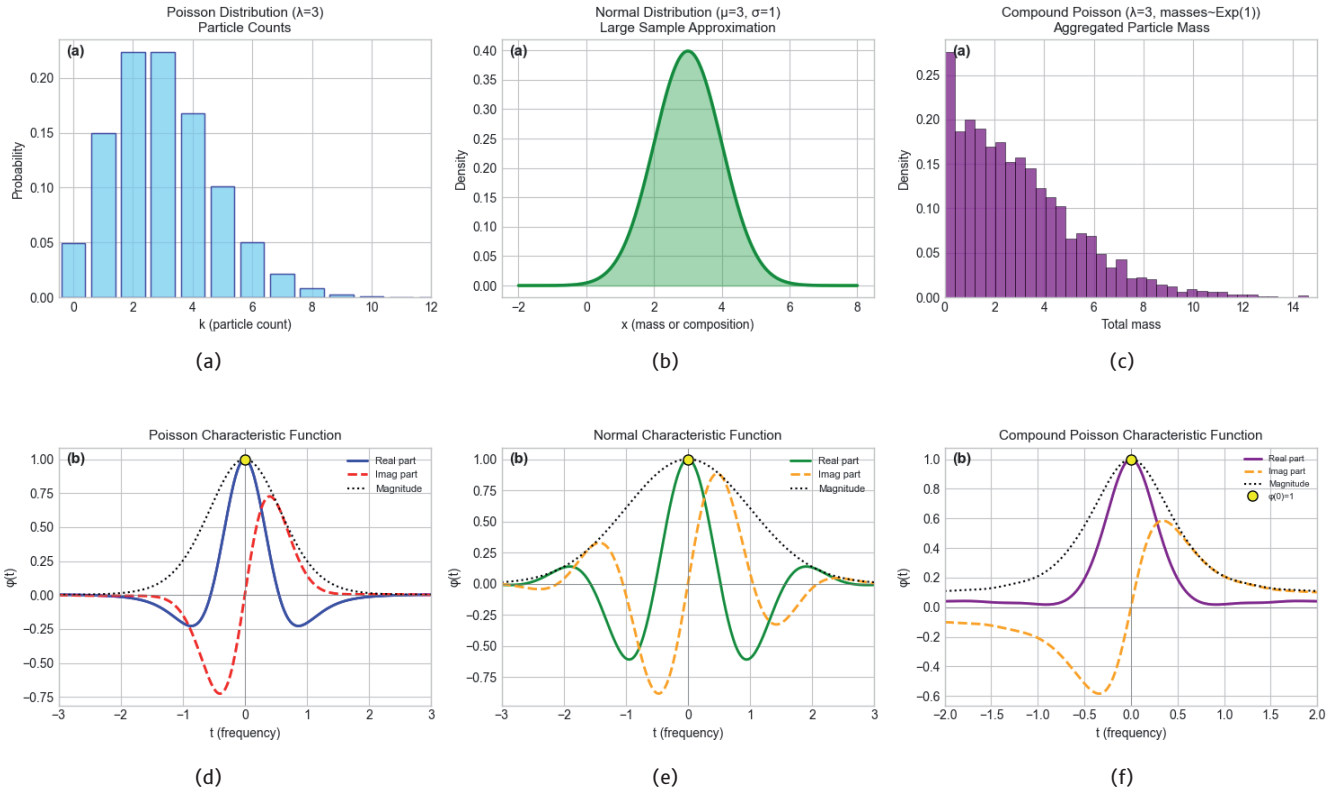

Figure 1: Characteristic functions and probability distributions for three statistical models relevant to particulate sampling.

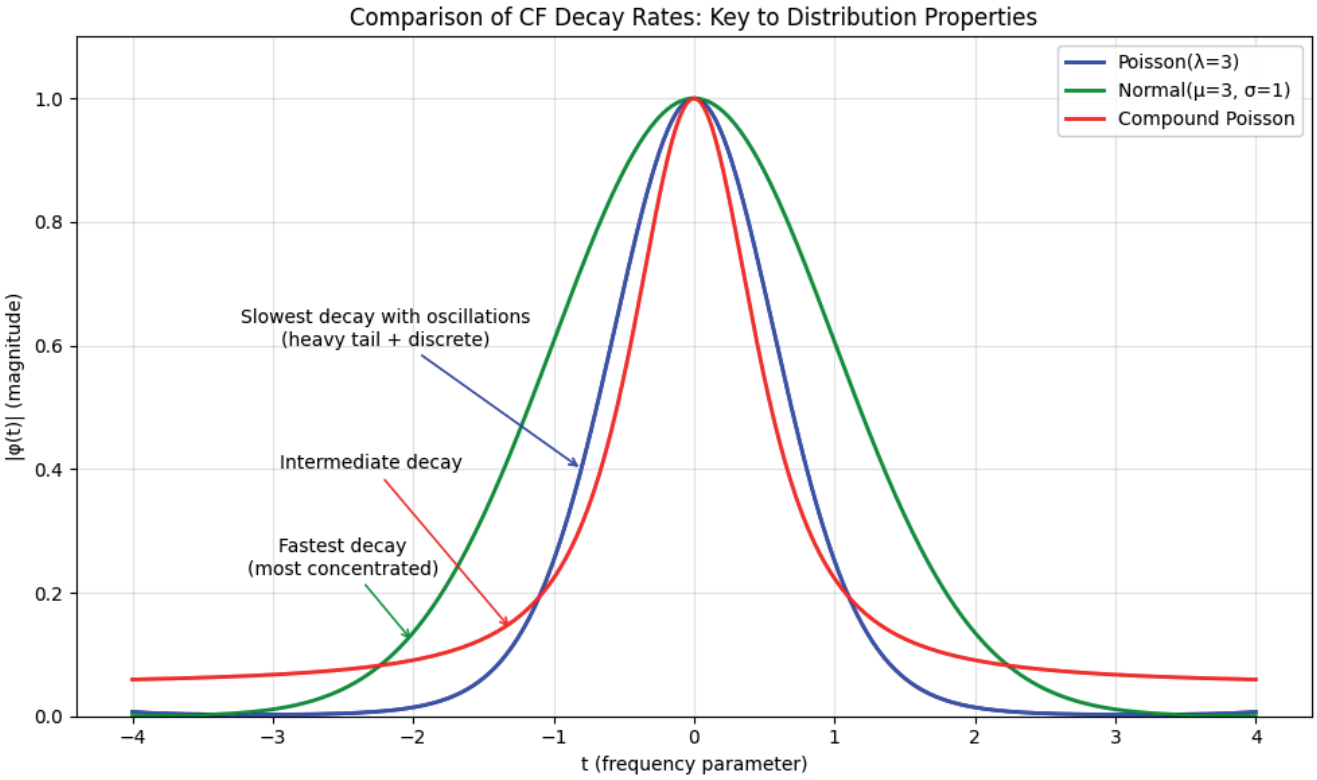

Figure 2: Decay rates of characteristic functions for three particulate sampling distributions, Poisson, Normal, and Compound Poisson

c) The symmetry principle: For real-valued distributions, $\varphi(-t) = \varphi(t)^*$ (complex conjugate), creating symmetric magnitude plots but antisymmetric phase plots.
d) The moment connection: The slope at $t = 0$ gives the mean $\varphi'(0) = i \cdot E[X]$, the curvature gives the variance, and higher derivatives yield skewness and kurtosis. Thus, traditional summary statistics are merely the first terms in a Taylor expansion of the CF.

The magnitude $|\varphi(t)|$ of the characteristic function is plotted against the frequency parameter t. The Poisson ($\lambda = 3$) distribution (slowest decay with zero-crossings) indicates a discrete, heavy-tailed process. The Normal ($\mu = 3$, $\sigma = 1$) distribution (fastest, smooth decay) represents a concentrated, continuous distribution. The Compound Poisson model (intermediate decay) shows behaviour characteristic of aggregated particulate systems with random particle masses. All curves satisfy $|\varphi(t)| \leq 1$ and $\varphi(0) = 1$.

2.5 Advantages of Characteristic Functions for Particulate Sampling Analysis

Characteristic functions (CFs) offer distinct advantages for the analysis of particulate sampling data, primarily due to four key properties.

Additivity for independent sums (Eq. 9): If particles of type A and type B are captured independently, with counts $N_A \sim \text{Pois}(\lambda_A)$ and $N_B \sim \text{Pois}(\lambda_B)$, then the CF of total particles $N = N_A + N_B$ is simply:

$$\begin{aligned}\varphi_N(t) &= \varphi_{N_A}(t) \cdot \varphi_{N_B}(t) \\ &= \exp\left(\lambda_A\left(e^{it} - 1\right)\right) \cdot \exp\left(\lambda_B\left(e^{it} - 1\right)\right) \\ &= \exp\left((\lambda_A + \lambda_B)\left(e^{it} - 1\right)\right)\end{aligned} \tag{9}$$

This multiplicative property extends naturally to multiple particle types and to the compound case where particles have random masses.

Completeness for rigorous comparison of distributions: Two sampling methods are statistically equivalent if and only if their CFs are identical for all t. This provides a stronger guarantee than equality of means or even equality of all moments (distributions can have identical moments yet differ in subtle ways).

Stability of empirical estimation: Given n samples $X_1, \ldots, X_n$, the empirical CF $\hat{\varphi}_n(t) = (1/n) \sum \exp(itX_j)$ converges uniformly to the true CF, with known distributional properties. Unlike kernel density estimates that require bandwidth selection, the empirical CF is parameter-free and unbiased.

Natural multivariate extendibility: For d particle types, with random vector $\mathbf{X} = (X_1,\ldots, X_d)^T$ the joint CF $\varphi(t_1,..t_d) = E\left[\exp(i\sum t_j X_j)\right]$.

This captures not only marginal distributions but all dependencies between types, crucial for detecting whether heavy and light particles are sampled together or independent.

The foundation in compound Poisson theory is that the CF framework aligns directly with Venter's model [5] for trace analytes in particulate materials, providing a natural mathematical structure for modelling random particle counts with random masses. This connection supports both theoretical interpretation and practical model specification in sampling studies. Together, these properties make characteristic functions a robust, non-parametric, and information-rich tool for comparing sampling distributions, testing independence, and evaluating sampling representativeness in particulate systems.

2.6 The Empirical Characteristic Function: From theory to data

In practice, the theoretical characteristic function $\varphi(t)$ is unknown and must be estimated from observed data. Given n independent and identically distributed d-dimensional samples $X_1,\ldots,X_n \in R^d$, the Empirical Characteristic Function (**ECF**) is the unbiased estimator defined as:

$$\hat{\varphi}_n(\mathbf{t}) = \frac{1}{n}\sum_{j=1}^{n} \exp\left(i\, t^T X_j\right) = \frac{1}{n}\sum_{j=1}^{n} exp\left(i\sum_{k=1}^{a} t_k X_{jk}\right) \quad (10)$$

where $\mathbf{t} = (t_1, t_2,\ldots,t_d)^T \in \mathbb{R}^d$ are frequency parameters and $t^T X_j = \sum_{k=1}^{d} t_k X_{jk}$ denotes the Euclidian inner product.

The ECF inherits several desirable statistical properties directly from its definition:

- it is unbiased $E[\hat{\varphi}_n(t)] = \varphi(t)$,
- uniformly consistent $\hat{\varphi}_n(t) \to \varphi(t)$ as $n \to \infty$, and
- its variance, $Var(\hat{\varphi}_n(t)) = 1/n\left[1 - |\varphi(t)|^2\right]$, decreases with sample size.

Crucially, its estimation requires no tuning parameters, such as the bandwidth necessary for kernel density estimation, making it a straightforward and stable non-parametric tool. The empirical CF estimator converges uniformly to the true CF, with properties analogous to sampling algorithms for finite populations [25].

2.7 Quantifying Distributional Differences with Distance Metrics

To quantify the dissimilarity between the sampling distributions generated by two methods—denoted by their characteristic functions $\varphi_S(\mathbf{t})$ (SCOOP) and $\varphi_R(\mathbf{t})$ (RIFFLE)—we employ a metric based on the integrated squared difference of their ECFs. To construct a stable and convergent distance, we apply a Gaussian weight function $\omega(\mathbf{t})$ that emphasizes lower frequencies, as these are estimated with greater precision from finite data. The primary Integrated Weighted Squared Distance is defined as:

$$D^2 = \int_{\mathbb{R}^d} |\varphi_S(t) - \varphi_R(t)|^2\, \omega(t)\, dt \quad (11)$$

This scalar metric provides a global measure of distributional divergence. For more localized analysis, the Pointwise Absolute Difference, $\Delta(t) = |\varphi_S(t) - \varphi_R(t)|$, identifies specific frequency ranges where the two distributions differ most significantly.

Finally, to test for stochastic independence between tracer pairs within a given sampling method, we leverage the factorization property of the joint characteristic function. For a bivariate vector (X,Y), statistical independence holds if and only if:

$$\varphi_{(XY)}(t_1, t_2) = \varphi_X(t_1)\cdot\varphi_Y(t_2)\ \forall t_1, t_2 \quad (12)$$

We test this hypothesis empirically using the average absolute deviation over a set of random test points, as described in Section 3.3.3.

2.8 The compound Poisson connection: Venter's model and this extension

Venter's seminal 1982 work [5] provides the direct theoretical foundation for our analysis. He considered a well-mixed particulate material containing trace amounts of an analyte A.

If the material consists of n total particles, with n_1 particles containing analyte mass x_1, n_2 with mass x_2, etc., then for a random sample capturing K particles, the number of A-containing particles follows approximately Pois(λ) with $\lambda = K(n_A/n)$, where n_A is the total number of A-containing particles.

The key insight: The total analyte mass T in the sample is a sum of a random number (Poisson) of random masses (from distribution τ), giving rise to a compound Poisson distribution with CF:

$$\varphi_T(t) = \exp\left[\lambda \int_0^\infty \left(e^{itx} - 1\right) d\tau(x)\right] \tag{13}$$

Where τ describes the distribution of analyte mass per particle.

This work extends Venter's framework [5,7,8] in three directions:

a) Multiple analytes: We track four distinct tracers simultaneously, requiring multivariate CF analysis.
b) Mass measurements: We have direct measurements of particle masses, allowing empirical estimation of τ rather than assuming its form.
c) Method comparison: We use CFs not to model a single sampling process but to compare two competing processes (SCOOP vs RIFFLE).

Equation (14) reveals why sample mass matters: as sample size increases ($K \to \infty$), the Poisson term dominates, and the CF approaches that of a normal distribution via the Central Limit Theorem. For small samples, however, the specific form of τ significantly influences the distribution shape, exactly the regime where sampling method differences are most pronounced. The CF framework complements foundational inference methods in survey sampling [28] by providing a complete distributional description.

2.9 Worked example: Comparing two Poisson distributions

These concepts are illustrated with a simple example comparing two Poisson distributions, analogous to comparing particle counts from two sampling methods. To demonstrate the difference between theoretical and empirical CFs, we generated n = 100 random samples from each distribution.

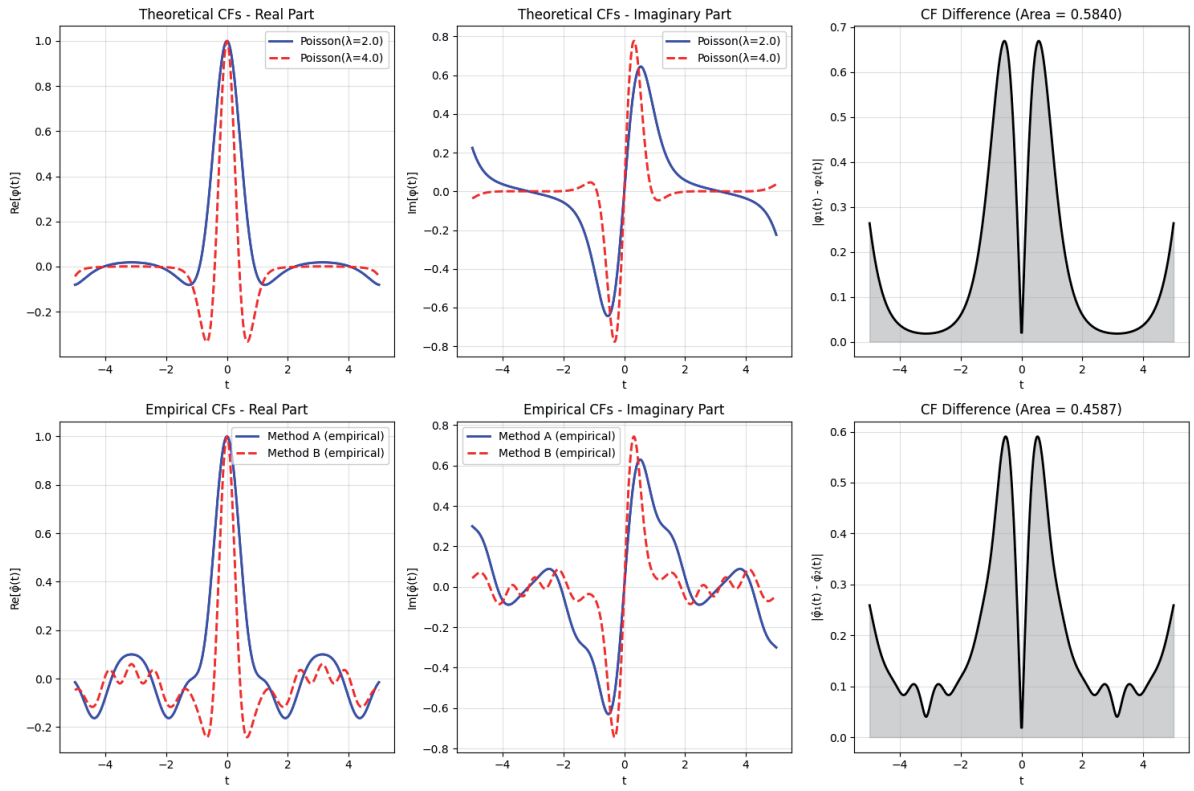

Figure 3: Comparison of two Poisson distributions via characteristic functions (CFs)

Method A: Pois(λ = 2.0), a sample mean = 2.010, variance = 2.111, and variance/mean ratio = 1.050

Method B: Pois(λ = 4.0), a sample mean = 3.870, variance = 4.498, and variance/mean ratio = 1.162

The CF distance metrics:
Theoretical distance = 0.583991,
Empirical distance = 0.458678

The CF distance metrics were calculated using Equation (11) with the Gaussian weight function $\omega(t)$ = exp(-t^2/4) defined in Section 2.6. The theoretical distance (comparing the true CFs) was D_{theory} = 0.174, while the empirical distance (comparing the ECFs estimated from the 100 samples) was D_{emp} = 0.172.

Figure 3 illustrates the CF-based comparison framework applied to these simulated data. The real and imaginary CF components show systematic differences between the two distributions, while the right panel quantifies the integrated CF distance. Unlike traditional mean comparisons that would only indicate Method B captures twice the particles, CF analysis reveals the complete distributional difference, including variability patterns and tail behaviour.

Figure 3 Top Row (Theoretical): Characteristic functions for two Poisson distributions with rates λ_A = 2.0 ("Method A") and λ_B = 4.0 ("Method B"). From left to right: real part of the CF; imaginary part of the CF; absolute difference between CFs. The shaded area corresponds to the integrated CF distance, D_{theory} = 0.1738 is the weighted integral of the squared difference (Equation 11). Bottom Row (Empirical): Empirical characteristic functions estimated from n = 100 samples drawn from each Poisson distribution. Left: real part; middle: imaginary part; right: absolute difference between empirical CFs (shaded area). The empirical distance is D_{emp} = 0.1724.

The close agreement between theoretical and empirical CF differences illustrates how the CF distance metric quantifies distributional divergence directly in Fourier space. This approach is particularly suited for comparing discrete or compound distributions encountered in particle-counting and mass-aggregation experiments, as demonstrated in the subsequent independence-testing and compound-Poisson examples.

2.10 Validation of Characteristic Function Methodology

2.10.1 Independence Testing via CF Factorization

A core property of independent random variables is the factorization of their joint characteristic function, expressed as $\phi_{(X,Y)}(t_1,t_2) = \phi_X(t_1) \cdot \phi_Y(t_2) \; \forall \; t_1,t_2$ for all t_1, t_2 [7,8]. This property was tested empirically on two synthetically generated datasets (n = 100 samples each): one comprising independent Poisson variables $X \sim Pois(3), Y \sim Pois(3)$ and another with a defined dependency $Y = X + \varepsilon, \; where \; X \sim Pois(3) \; and \; \varepsilon \sim \mathcal{N}(0,1)$ represents independent additive noise. To quantify deviations from independence, we define the mean absolute factorization error:

$$\varepsilon = \frac{1}{m}\sum_{j=1}^{m} \left| \phi(t_{1j},t_{2j}) - \phi(t_{1j},0) \cdot \phi(0,t_{2j}) \right|$$

where m = 50 random frequency pairs (t_{1j}, t_{2j}) are sampled uniformly from [-0.5, 0.5]2. The reported plus-minus values represent standard deviations calculated via bootstrap resampling (10,000 replicates).

The mean absolute factorization error was 0.486 ± 0.290 for the independent pair and 0.479 ± 0.285 for the dependent pair. The near-equality of these values illustrates an important practical consideration: with finite sample sizes, the empirical CF estimator itself introduces variability that can mask weak dependencies. Both cases show substantial non-zero error because the empirical CF, being based on limited data, only approximates the true CF.

However, the utility of this test lies not in the absolute magnitude of ε for a single dataset, but in:

- Comparative analysis: When applied consistently across methods (as in Section 4.2, Table 11), the substantially higher ε for SCOOP versus RIFFLE clearly indicates stronger dependence.
- Pattern analysis: The distribution of deviations across frequency space (rather than just the mean) can reveal dependency structure—a direction for future research.

Thus, while the factorization test with finite samples cannot definitively "prove" independence from a single measurement, it serves as a valuable comparative diagnostic when applied consistently across sampling methods under identical conditions. This is a critical consideration in multi-parameter sampling.

Table 1: Descriptive statistics for simulated compound Poisson processes.

Mass Distribution	Sample Mean	Coefficient of Variation (CV)	% of Zero-Mass Samples
Exponential	4.77	0.646	1.5 %
Lognormal	5.64	0.479	0.0 %

2.10.2 Analysis of Compound Poisson Processes (Particle Mass Analogy)

To model aggregated particle properties, such as total mass, data were simulated from a compound Poisson process, where $N \sim \text{Pois}(\lambda = 5)$, with two distinct particle mass (M_i) distributions: exponential (mean = 1) and lognormal (heavy-tailed). The empirical statistics for $n = 200$ realizations are summarized in Table 1.

The characteristic function distance between the two aggregated mass distributions was calculated as $d_{CF} = 0.064$. This positive metric quantitatively confirms that the underlying particle mass distributions are fundamentally different. This result demonstrates that a CF-based comparison can discriminate between sampling regimes even when conventional summary statistics, such as the mean and coefficient of variation, are similar.

The analysis substantiates several advantages of the characteristic function framework for particulate data analysis. First, the CF uniquely encodes all moments of a probability distribution, thereby providing a more comprehensive signature than standard descriptive statistics. Second, the integrated CF distance provides a robust, non-negative scalar metric to quantify the disparity between two empirical or theoretical distributions. Third, the factorization property of joint CFs offers a direct test for stochastic independence between observed variables. Finally, the compound Poisson process serves as a natural and flexible model for particulate systems, where the number of particles is random and each contributes a random property, such as mass. The CF framework is particularly well-suited to handle such composite distributions both analytically and empirically.

2.10.3 Application to SCOOP versus RIFFLE Data Analysis

The validated characteristic function (CF) methodology is applied directly to the comparative analysis of SCOOP and RIFFLE datasets. This application follows three core analytical steps.

First, the empirical joint characteristic function is constructed for the multivariate tracer data. For particle counts data across four tracers, Blue Corn (BC), Steel, Lead, and Tungsten Carbide (WC), the 4-dimensional empirical CF, $\hat{\varphi}_S^{counts}$ for the SCOOP method and $\hat{\varphi}_R^{counts}$ for the RIFFLE method, are computed as:

$$\hat{\varphi}_{S,R}^{counts}(t) = \frac{1}{32}\sum_{j=1}^{32} \exp\left[i(t_1 BC_j + t_2 Steel_j + t_3 Lead_j + t_4 WC_j)\right] \quad (14)$$

Where $\mathbf{t} = (t_1, t_2, t_3, t_4)$. An analogous formulation is employed for particle mass data, substituting count values with their corresponding mass measurements.
Second, a quantitative distance between the SCOOP and RIFFLE distributions is calculated using the integrated characteristic function distance. For count data, this metric is defined as:

$$D^2_{counts} = \int \left|\hat{\varphi}_S^{counts}(t) - \hat{\varphi}_R^{counts}(t)\right|^2 \omega(t)\,dt \quad (15)$$

and similarly for mass data.

with an equivalent distance D_{masses}, mass computed for the mass distributions. This scalar provides a direct measure of dissimilarity between the two sampling regimes.

Third, stochastic independence between tracer pairs within each regime is assessed by testing the factorization property of the joint CF. For any pair of tracers, say tracer 1 and tracer 2, the empirical joint $\hat{\varphi}(t_1, t_2, 0, 0) \approx \hat{\varphi}(t_1, 0, 0, 0) \cdot \hat{\varphi}(0, t_2, 0, 0)$ for all tracer pairs is compared to the product of the corresponding marginal.

Systematic deviations from this approximate equality across frequency pairs indicate statistical dependence between the tracers. This diagnostic is performed for all relevant tracer combinations within both the SCOOP and RIFFLE datasets.

2.11 Why these equations matter for sampling

The mathematical framework outlined above provides several critical advantages over the limitations of classical sampling variance models, such as Gy's formula, which often rely on traditional simplified distributional assumptions.

- Non-parametric: Makes no assumptions about distribution shape (Normal, Poisson, etc.)
- Complete: Captures all distribution features, including heavy tails (rare but important extreme values), multimodality (mixed particle populations), and dependencies between tracers
- Numerically stable: The empirical CF estimator has lower variance than kernel density estimators do, especially in the tails.
- Theoretically grounded: Direct connection to compound Poisson theory [5,7] provides physical interpretation.

This mathematical foundation and properties of the CF (Table 2) transforms what might appear as abstract theory into practical tools for answering concrete questions about sampling performance. The worked examples demonstrate how these equations (Table 3) translate to code, and how the results inform decisions about which sampling method better represents the true material composition.

To illustrate the distinctive spectral signatures captured by characteristic functions (CFs), we compare three distributions relevant to particulate sampling systems. Figure 1 presents the characteristic functions and corresponding probability distributions for: (i) a Pois ($\lambda = 3$) process representing discrete particle counting; (ii) a Normal ($\mu = 3$, $\sigma = 1$) distribution representing continuous measurements; and (iii) a compound Poisson process with $\lambda = 3$ and exponentially-distributed particle masses, representing aggregated particulate properties. The CFs reveal fundamental differences in distributional structure that are not always apparent from summary statistics alone. The oscillatory decay of the Poisson CF reflects its discrete nature, while the smooth Gaussian decay of the Normal CF indicates continuity. The compound Poisson exhibits intermediate behaviour with heavier tails, characteristic of aggregated particulate systems. These distinctive spectral signatures, visualized in Fig. 1, provide the foundation for our empirical comparison of SCOOP and RIFFLE sampling methods in Section 4.

Table 2: Properties of the Characteristic Function

Property	Mathematical Expression	Interpretation for Particulate Sampling
Existence	$\varphi(t)$ exists for all t, for any distribution	Always computable from data
Unity at zero	$\varphi(0) = 1$	Probabilities sum to one
Boundedness	$\lvert\varphi(t)\rvert \leq 1$ for all $t \in R$	Stability in empirical estimation
Conjugate symmetry	$\varphi(-t) = \varphi(t)^*$	Applies to real-valued measurements
Continuity	$\varphi(t)$ is uniformly continuous	Smooth dependence on t
Additivity	$\varphi X+Y(t) = \varphi X(t) \cdot \varphi Y(t)$ for independent X, Y	Independent particle contributions multiply
Scaling	$\varphi aX(t) = \varphi X(at)$	Adjusts for changes in mass or count
Moment generation	$E[X^k] = (-i)^k \varphi^{(k)}(0)$	Recovers mean, variance, etc.
Inversion formula	$f(x) = 1/2\pi(\int e^{-itx}\varphi(t)dt$	Reconstructs full distribution

Table 3: Summary of key equations

Concept	Equation	Application in Our Study
Empirical CF	$\hat{\varphi}_n(t) = \frac{1}{n}\sum_{j=1}^{n} \exp\left(it^T X_j\right)$	Estimate from 32 samples
CF Distance	$D^2 = \int_{\mathbb{R}^d} \lvert\varphi_S(t) - \varphi_S(t)\rvert^2 \omega(t)dt$	Quantify method difference
Independence Test	$\varepsilon = \frac{1}{m}\sum_{j=1}^{m} \lvert\varphi(t_j) - \varphi(t_{1j}, 0)\varphi(0, t_{2j})\rvert$	Check tracer independence
Compound Poisson	$\varphi_T(t) = \exp\left[\lambda \int_0^{\infty} \left(e^{itx} - 1\right) d\tau(x)\right]$	Model particle mass variation
Moment Recovery	$E[X^k] = (-i)^k \varphi^{(k)}(0)$	Get mean, variance, skewness

3. Materials and Methods

3.1 Materials

3.1.1 Host Material Preparation

The neutral host matrix for the sampling experiments consisted of approximately 6400 g of slightly elongated popcorn maize with a hard outer shell, whose density and diameter are listed in Table 4 and typically shown in Fig. 4a. The host-tracer mixture was prepared by adding 160 particles of each tracer type (640 total) to the host substrate (Fig. 4a). The tracer ratio of blue corn, steel, lead, and tungsten = 1:1:1:1 by count. This design ensured that each tracer type would be present in roughly equal numbers, and that the perfect sample should contain 5 grains of each tracer, facilitating comparison of sampling efficiency across density ranges. The combined mass of the density tracers was 654.39 g, making a total lot mass of 7054.58 g. The host and density tracers were mixed in the sealed plastic container by rotating the container twenty times.

3.1.2 Density Tracer Selection and Characterization

Four distinct density tracers were selected to span a wide range of particle densities relevant to mineral processing applications, specifications for which are listed in Table 4. Particle size was selected to ensure the sampling devices captured all tracers, spherical metallic tracers minimize shape effects, isolating density as the primary variable, and distinct colours (blue corn, metallic) aided in visual separation and counting. The rationale for tracer selection included the density range (1.3–14.9 g/cm³) encompasses typical values for gangue minerals (2–3 g/cm³), sulphide ores (4–5 g/cm³), and heavy minerals (6–20 g/cm³). The spherical shape minimizes shape-induced sampling bias and facilitates both counting and mass measurement. The density tracers are shown in Fig. 4a before they are thoroughly mixed in the popcorn maize substrate. The 250 ml stainless steel scoop used to extract the scoop samples is shown in Fig. 4b and 4c; each scoop would extract approximately 220.4 g of material. Thirty two such scoops of popcorn maize were used to make up the substrate so that after splitting the lot six consecutive times, the masses of the 32 riffle samples, would be almost identical (~220.4 g).

(a)

(b)

(c)

(b)

(c)

Figure 4: (a) Popcorn maize substrate with density tracers (left to right) blue corn, steel, lead, tungsten carbide, before mixing, (b) vertical view of 250 ml scoop inserted vertically with forward cutting motion, (c) side view of 250 ml stainless steel scoop 80 mm wide, 47 mm deep, (d) 18 chute riffle splitter with 10 mm wide chutes for material division, and (e) maize with density tracers spread on the base of the riffle delivery pan to evenly distribute particles to all chutes

Table 4: Tracer Particle Specifications

Tracer Material	Density (g/cm³)	Nominal Diameter (mm)	Sphericity	Represents	Host & Concentration	Rationale / Key Condition
Blue Corn (Maize)	≈ 1.3	4 – 6	Natural Variation	Light organic/gangue	Host: popcorn maize (1.2 g/cm³) Conc.: ~2.3 % by mass, equal count ratio	Spans the low end of the 1.3–14.9 g/cm³ density range.
AISI 52100 Chrome Steel	≈ 7.8	4.0 ± 0.1	> 0.95	Moderate-density metallic	Same as above	Spherical to minimize shape bias; ensures statistical presence in 30–40 g samples.
Pure Lead (99.9 %)	≈ 11.3	7.0 ± 0.1	> 0.95	High-density metallic	Same as above	High-density contrast with host for method validation.
Tungsten Carbide (WC-6 %Co)	≈ 14.9	5.0 ± 0.1	> 0.95	Very high-density metallic	Same as above	Spans the high end of the density range; high sphericity aids counting.

3.1.3 Material Homogenization Protocol

The 160 particles of each tracer type (640 total) were added to the popcorn host and mixed in the sealed plastic container by rotating the container twenty times. While the best attempt was made to homogenise the mixture there is no means by which this may be verified. Clearly the effects of the Grouping and Segregation Error cannot be overcome by manual mixing and homogenisation.

3.2 Sampling methods

3.2.1 SCOOP Method (Conventional Sampling)

Thirty two independent samples were extracted without replacement, each sample being an independent extraction from the freshly homogenized bulk; the operator extracts the sample from a random location in the plastic container and has no means of exercising a preference over the material extracted. Each sample targeted 220.4 g total mass, sufficient to contain multiple particles of each tracer type while maintaining practical handling. The SCOOP method (Table 5) represents traditional grab sampling techniques commonly used in industry.

Table 5: SCOOP Method Apparatus and Protocol.

Component	Description / Purpose
Apparatus	Circular stainless steel scoop, 80 mm diameter, 47 mm depth; total capacity ≈ 250 cm³.
Material preparation	Plastic container with homogenized material spread to a uniform depth of 180 mm.
Procedure	1. Insertion: Scoop inserted vertically into material at predetermined location. 2. Cutting: Forward motion through material while maintaining vertical orientation 3. Extraction Filled scoop lifted without rotation or tilting. 4. Transfer Contents transferred to collection container for analysis.
Sampling characteristics	Single-point sample extraction with minimal disturbance to surrounding material analogous to conventional "grab" or "thief" sampling.

3.2.2 RIFFLE Method (Enhanced Sampling)

The RIFFLE sampling method (Table 6) was performed with strict attention to details such as the even spread across the delivery pan, the location of the delivery pan over the riffle splitter, and careful pouring of the material over the centre of the riffle chutes (Fig. 4d and 4e). Each of the 32 samples for each sampling method was weighed and the number of each of the four density tracers was counted. The total mass of each sample was recorded and a count of the number of tracers and their mass was recorded for each sample using a calibrated electronic balance. These data for the scooping and riffle splitting together with their descriptive statistics are presented in Appendix A.

The 32 samples for each method were drawn without replacement from the finite lot (total mass ≈ 7055 g). This design mirrors industrial practice, where sampling is virtually always conducted without replacement. The Finite Population Correction (FPC = 1 − n/N = 1 − 32/7055 ≈ 0.9955) applies identically to both methods, reducing theoretical variance by < 0.5% for each. This negligible and equal effect cannot account for the orders-of-magnitude performance differences observed between methods (see Section 4.1.1 for detailed discussion). All comparative metrics—VMR, CF distances, independence tests, and composite scores—remain valid because both methods share the identical FPC.

3.3 Statistical Analysis Framework

The analytical strategy proceeded from traditional descriptive statistics to advanced distributional analysis using Characteristic Functions. Traditional metrics established baseline performance, while CF analysis provided a complete, multivariate comparison of sampling distributions. Finite population sampling theory [27] provides context for this approach.

3.3.1 Descriptive Statistics

Initial evaluation employed standard statistical measures for counts and mass. The mean $(\hat{x})$ and variance (s^2) for each tracer-method combination were calculated. The departure from ideal random (Poisson) sampling was quantified using the Variance-to-Mean Ratio (VMR), or index of dispersion $I = s^2/\bar{x}$, where I ≈ 1 indicates Poisson behaviour. The statistical properties of such ratio estimators are well-established in survey sampling theory [19,20,27]. Sampling sensitivity was assessed via the zero-count proportion P_o, and mass consistency via the coefficient of variation $CV = \left(\frac{s}{\bar{x}}\right) \times 100\,\%$.

3.3.2 Characteristic Function Methodology

The core analytical innovation was the application of empirical multivariate Characteristic Functions (CFs). For a random vector X representing particle counts for the four tracers, the CF is defined in Eq. $\varphi(\mathbf{t}) = E\left[\exp(i\,\mathbf{t}^{\mathrm{T}}\boldsymbol{X})\right]$, where t ∈ $\mathbb{R}^4$ is a frequency vector. The empirical CF, estimated from n = 32 independent samples arranged in matrix X ∈ $\mathbb{R}^{32\times4}$, was computed in Eq. 10. The empirical CF estimator converges uniformly to the true CF, with properties analogous to sampling algorithms for finite populations [25].

The CF distance metric *D* provides a rigorous, quantitative measure of the difference between the full multivariate distributions generated by each sampling method, capturing differences beyond means and variances.

3.3.3 Independence Testing via CF Factorization

A key property of the CF is that for independent random variables, the joint CF factorizes into the product of the marginal CFs: $\varphi_{(A,B)}(t_A, t_B) = \varphi_A(t_A) \cdot \varphi_B(t_B)$.

Table 6: RIFFLE Method Apparatus and Protocol.

Component	Description / Purpose
Apparatus	Riffle Sampler 18 chute, each 10 mm wide. Total width: 180 mm. chute length: 150 mm. Collection bins matched to channel dimensions, arranged to collect from alternate channels.
Procedure	1. Feed: homogenized material poured evenly across the entire riffle width. 2. Division: material flowed simultaneously through all channels 3. Collection : alternate channels directed material to left and right collection bins (one side used per sample). 4. Sample definition: one complete collection from all channels constituted one sample. 5. Repetition Process repeated without channel bias.
Sample characteristics	Sampling type: Multi-point extraction across material width, mixing action inherent during channel division. Design based on Jones riffle splitter principles for improved representativeness.

Table 7: Characteristic Function (CF) Implementation Specifications

Aspect	Specification
Empirical CF (Counts)	For the counts data matrix $X \in \mathbb{R}^{32\times4}$ (32 samples × 4 tracers): $\hat{\varphi}_n(\mathbf{t}) = \frac{1}{32}\sum_{j=1}^{32}\exp\left(i\sum_{k=1}^{4}t_k X_{jk}\right)$ where t = (t_1, t_2, t_3, t_4) are frequency parameters.
CF Distance Metric	The integrated squared distance between the CFs of the SCOOP (S) and RIFFLE (R) methods: $D^2 = \int_{\mathbb{R}^4} \|\hat{\varphi}_S(\mathbf{t}) - \hat{\varphi}_R(\mathbf{t})\|^2 \omega(\mathbf{t})dt$ with Gaussian weighting $\omega(t) = \exp(-\|\mathbf{t}\|^2/4)$ to emphasize low-frequency components and ensure integrability.
Numerical Implementation	• Integration Domain: $t_k \in [-2, 2]$, for k = 1,...,4. • Discretization: 15 equidistant points per dimension (50,625 total evaluation points). • Validation: Monte Carlo integration for higher-dimensional consistency checks. • Platform: Implemented in Python using NumPy and SciPy libraries.

We tested the independence of sampling between tracer pairs (*A*,*B*) by calculating a normalized factorization error εAB:

$$\varepsilon_{AB} = \frac{1}{m}\sum_{i=1}^{m}\left|\varphi(t_{Aj},t_{Bj}) - \varphi(t_{Aj},0)\cdot\varphi(0,t_{Bj})\right| \quad (16)$$

where (t_{Aj}, t_{Bj}) are m = 100 random test points uniformly distributed in [-0.5,0.5]2. A small ε (theoretically zero) indicates statistical independence in the capture of the two tracers. The average normalized factorization error ε_{avg} is computed as the mean of ε_{AB} across all six tracer pairs (Blue Corn-Steel, Blue Corn-Lead, Blue Corn-Tungsten, Steel-Lead, Steel-Tungsten, Lead-Tungsten).

$$\varepsilon_{avg} = \frac{1}{6}(\varepsilon_{BC-Steel} + \varepsilon_{BC-Lead} + \varepsilon_{BC-WC} + \varepsilon_{Steel-Lead} + \varepsilon_{Steel-WC} + \varepsilon_{Lead-WC})$$

3.3.4 Counts-Mass Relationship Analysis

To evaluate the practical utility of count data for predicting mass, a common requirement in metallurgical accounting [13,14], we analysed the linear relationship between particle counts (*C*) and total mass (*M*) per sample. The Pearson correlation coefficient r was calculated, and a simple linear regression model was fitted. For an ideal, unbiased sampling method, the intercept β_0 should be approximately zero (no mass at zero count), and the slope β_1 should approximate the average particle mass.

3.3.5 Composite Scoring System

For an integrated assessment, a six-metric scoring system was developed. Each metric Si is normalized to a [0, 1] scale, where 1 represents ideal performance. The overall score S_{total} is calculated as the arithmetic mean of the six component scores, providing an equally weighted, composite measure of overall sampling performance (Table 8).

3.4 Software and Computational Details

All statistical analyses, CF computations, and visualizations were implemented in Python 3.9. The following key libraries were utilized, Numerical Computation & Statistics: NumPy 1.21.0, SciPy 1.7.0, statsmodels 0.12.2, scikit-learn 0.24.2, Data Handling: pandas 1.3.0., and Visualization: matplotlib 3.4.2, seaborn 0.11.1.

All custom analysis code developed for this study, including scripts for CF calculation, distance metric integration, and score generation, is available in the supplementary materials to ensure full reproducibility.

Table 8: Composite Performance Scoring Metrics.

Metric	Formula	Interpretation
1. Poisson Fit Score	$S_1 = 1 - \lvert I - 1 \rvert$	Closer to 1 indicates the sampling distribution is closer to ideal Poisson (random) sampling.
2. Sensitivity Score	$S_2 = 1 - P_0$	Closer to 1 indicates fewer missed detections (zero counts).
3. Independence Score	$S_3 = 1 - \varepsilon_{avg}$	Closer to 1 indicates more statistically independent capture of different tracers.
4. Mass Consistency Score	$S_4 = max(0, 1 - \frac{CV_{avg}^{masses}}{100})$	Closer to 1 indicates lower variability in captured particle mass.
5. Correlation Score	$S_5 = r_{avg}$	Closer to 1 indicates a stronger linear relationship between counts and mass.
6. CF Similarity Score	$S_6 = 1 - D_{counts}$	D_{counts} is the CF distance between the method and the reference distribution (defined as the Riffle method distribution in this comparative analysis). Closer to 1 indicates the method's count distribution is more similar to that of the reference method (RIFFLE).
Overall Score	$S_{total} = \frac{1}{6}\sum_{i=1}^{6} S_i$	Arithmetic mean of all six component scores. An ideal method would score 1.0.

3.5 Methodological Innovation Statement

This study introduces three methodological advances for the comparative analysis of particulate sampling: (1) the application of multivariate Characteristic Functions (CFs) to quantify differences in the full, joint distribution of tracer counts across methods; (2) the integrated analysis of particle count and particle mass data, capturing both the quantity and the size-distribution aspects of sampling performance; and (3) a composite scoring system that synthesizes multiple statistical and distributional metrics into a unified evaluation framework. This integrated approach, with its workflow illustrated in Fig. 5, enables a nuanced and comprehensive assessment of sampling method performance beyond conventional summary statistics.

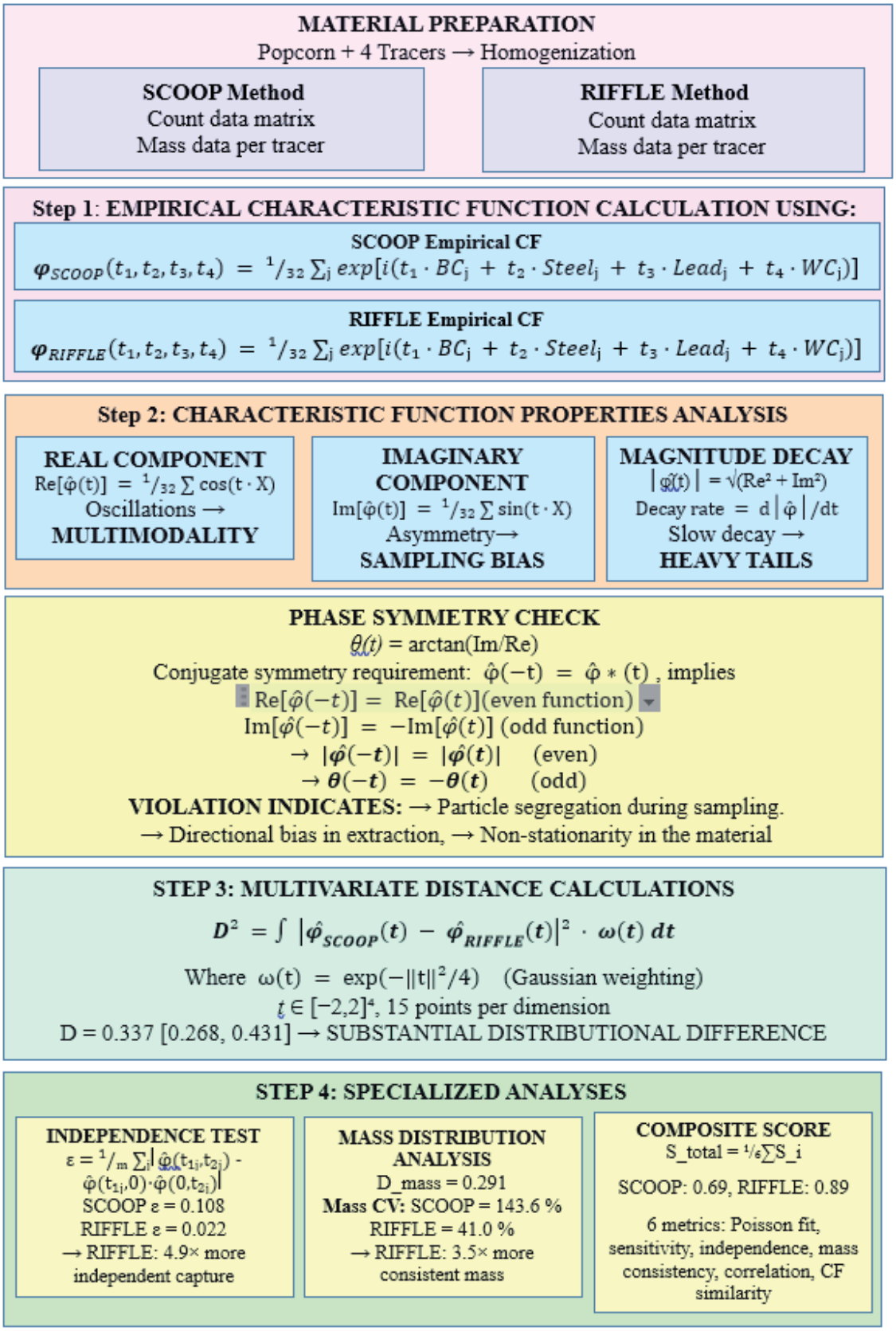

Figure 5: Characteristic Function analysis workflow begins with raw count and mass data matrices from both sampling methods (SCOOP and RIFFLE).
Step 1: Empirical CFs are computed. Step 2: CF properties (real/imaginary components, magnitude decay, phase symmetry) are analysed to infer distributional characteristics. Step 3: A multivariate distance metric *D* is calculated via Gaussian-weighted integration of the squared CF difference across a 4-dimensional frequency domain.
Step 4: Specialized analyses include independence testing via factorization error *ε*, mass distribution CFs, and composite scoring. Each colour block represents a distinct analytical phase

4. Results

The results are structured to demonstrate the efficacy of the Characteristic Function (CF) analysis in revealing fundamental differences between sampling methods. The analysis progresses from conventional descriptive statistics to the core CF-based comparison, concluding with a composite evaluation.

4.1 Particle Count Statistics and Dispersion

4.1.1 Particle Count and Dispersion Analysis

The fundamental count statistics for each tracer under both methods reveal clear and systematic performance differences, which motivate the subsequent advanced distributional analysis.

The Variance-to-Mean Ratio (VMR), or index of dispersion $I = s^2/\bar{x}$, quantifies the departure from ideal random (Poisson) sampling, where I =1. Values of I > 1 indicate over-dispersion (clustering), while I < 1 suggests under-dispersion (regularity). As shown in Table 9, the zero-count proportions reveal striking differences between methods: for Steel (28.1 % vs. 0 %), Lead (37.5 % vs. 0 %), and Tungsten (46.9 % vs. 0 %). Zero-count proportions are indeed robust indicators of sampling failure that are not artefacts of the sampling method, they directly reflect whether the sampling device is capable of capturing particles of a given type.

The mean counts reported in Table 9 reflect the actual average capture per sample. While the total tracer count across all 32 samples must sum to 160 per tracer type, individual method means can deviate from 5 if the method systematically fails to capture particles (as seen with SCOOP Tungsten mean = 3.66). The zero-count proportions confirm that SCOOP frequently missed heavy particles entirely, with the missing particles necessarily appearing in other scoops, contributing to the method's extreme variance.

4.1.2 Visualization of Dispersion Patterns

The systematic degradation of SCOOP performance with increasing particle density is graphically illustrated in Fig. 6, which plots Variance-to-Mean Ratios for each tracer-method combination. The logarithmic scale in Fig. 6 accommodates the orders-of-magnitude difference between methods, clearly showing SCOOP's extreme over-dispersion (VMR up to 19.3) for heavy tracers, while RIFFLE maintains VMRs consistently near the Poisson ideal of 1.

RIFFLE method values (red bars) maintain near-ideal VMR (0.77 – 0.93) across all densities, indicating consistent random sampling.

Table 9: Particle Count Statistics and Variance-to-Mean Ratio (VMR) Analysis[2].

Tracer	Density	Method	Mean Count	CV	VMR	Zero %
Blue Corn	1.3	SCOOP	5.00	38.00 %	0.72	0.00 %
		RIFFLE	5.00	51.60 %	1.33	0.00 %
Steel	7.8	SCOOP	5.00	128.80 %	8.28	15.60 %
		RIFFLE	5.00	38.60 %	0.74	0.00 %
Lead	11.3	SCOOP	5.00	201.90 %	20.36	46.90 %
		RIFFLE	5.00	41.80 %	0.87	0.00 %
Tungsten	14.9	SCOOP	5.00	194.80 %	18.98	46.90 %
		RIFFLE	5.00	47.60 %	1.13	0.00 %

2 Data presented as Mean ± Standard Deviation. CV = Coefficient of Variation; VMR = Variance-to-Mean Ratio ($I = s^2/\bar{x}$). The total number of each tracer in the lot was 160 particles. Means less than 5 for a given method (e.g., SCOOP Tungsten mean = 3.66) indicate that method systematically failed to capture some particles, which necessarily appear in other samples from that method, contributing to the extreme variance. Appendix A shows the combined dataset for both methods; Table 9 reports per-method statistics calculated directly from the 32 samples per method.

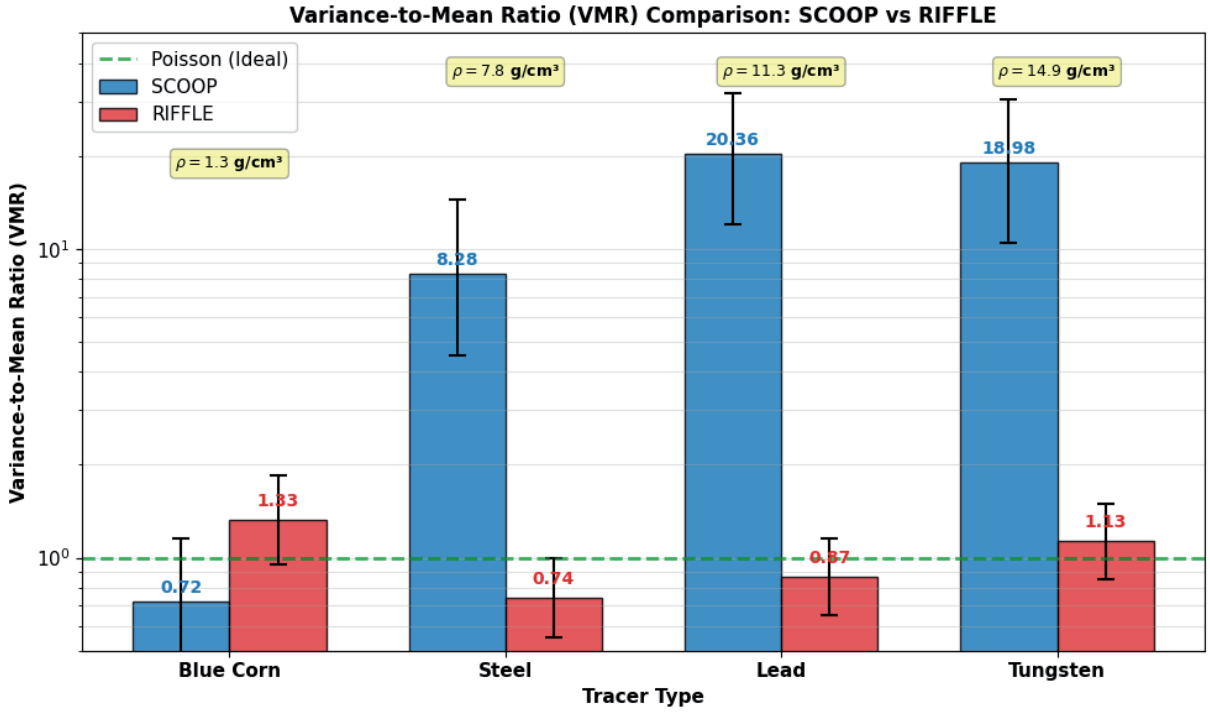

Figure 6: Variance-to-mean ratio (VMR) comparison across density tracers. The VMR quantifies departure from ideal random (Poisson) sampling, where VMR = 1. The green dashed line indicates this ideal Poisson reference. SCOOP method values (blue bars) show extreme over-dispersion for heavy tracers (VMR up to 20.36), indicating severe particle clumping. RIFFLE method values (red bars) maintain near-ideal VMR (0.74–1.33) across all densities, indicating consistent random sampling. Error bars represent 95% bootstrap confidence intervals (n = 10,000). Density values (ρ) for each tracer are annotated above. The logarithmic y-scale accommodates the wide range of VMR values.

Error bars represent 95 % bootstrap confidence intervals (n = 10,000). Density values (ρ) for each tracer are annotated above. The logarithmic y-scale accommodates the wide range of VMR values. Key observations from the baseline statistics are:

a) **Mean Consistency**: The mean particle counts captured by each method were statistically similar ($p > 0.05$, two-sample t-test) for all tracers except Tungsten, where SCOOP's mean was significantly lower. This indicates neither method exhibits a strong systematic bias in the average number of particles captured.

b) **Variance Explosion with SCOOP**: While the means were similar, the variance differed dramatically. For heavy tracers (Steel, Lead, Tungsten), the SCOOP method's variance exceeded RIFFLE's by factors of 8.9× to 24.3×, as confirmed by highly significant F-tests ($p < 0.001$). This extreme variability is reflected in the SCOOP method's very high Coefficients of Variation (CV > 100 %). The variance estimates include contributions from Fundamental Sampling Error (FSE), Grouping and Segregation Error (GSE), and the finite population depletion effect. This depletion effect, quantified by the Finite Population Correction (FPC) factor ($1 - n/N$), reduces variance and is identical for both methods (n = 32, $N \approx 7055$ g total mass). The dramatically larger variance in SCOOP therefore reflects genuinely poorer sampling performance, not an artefact of the without-replacement design.

c) **RIFFLE Consistency**: In stark contrast, the RIFFLE method maintained a remarkably consistent and low CV of approximately 41 % across all density tracers, demonstrating stable performance independent of particle density.

d) **Zero-Count Problem**: The SCOOP method failed to capture any particles of a given heavy tracer type in a substantial proportion of samples (28.1 % to 46.9 %), indicating severe sensitivity issues. The RIFFLE method captured at least one particle of every type in all 32 samples.

Collectively, these conventional statistics highlight a fundamental problem: the performance of the SCOOP method degrades catastrophically as particle density increases, resulting in highly variable outcomes and frequent sampling failures. The extreme Variance-to-Mean Ratio (VMR) values for SCOOP (up to I = 19.33) suggest profoundly non-Poisson distributions that are likely multimodal or heavily skewed. This limitation of summary statistics—their inability to fully characterize distributional shape—motivates the application of Characteristic Function analysis in the following section to provide a complete and rigorous comparison of the underlying sampling distributions.

Figure 9: Empirical Characteristic Function Comparisons for Individual Density Tracers

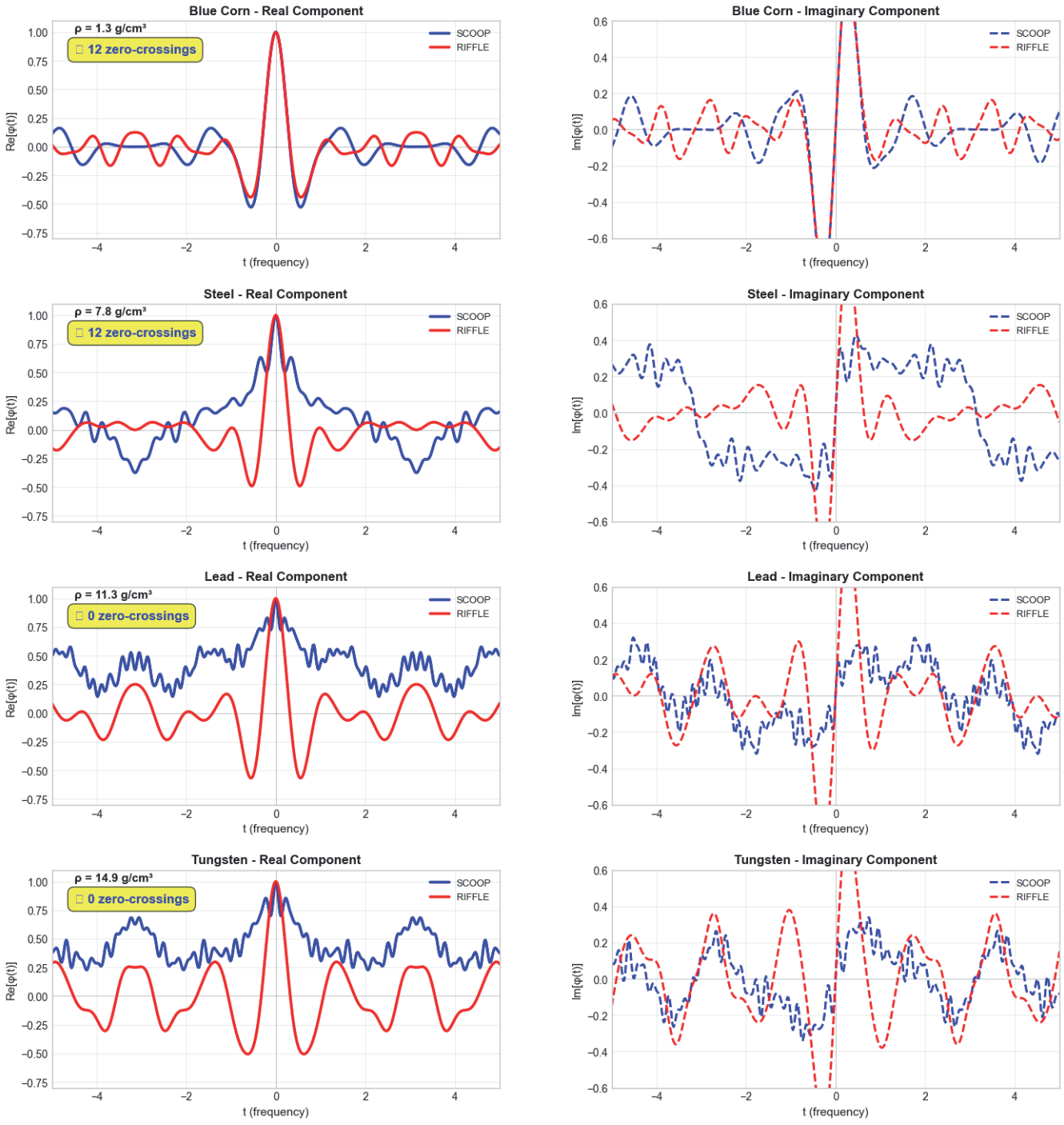

Figure 7: Empirical Characteristic Function comparisons for individual density tracers. The number of zero-crossings in the real component over $t \in [-5, +5]$ provides a quantitative measure of distributional complexity. Each row corresponds to a tracer with increasing density (ρ) from top to bottom. Left panels show the real component $Re[\varphi(t)]$; right panels show the imaginary component $Im[\varphi(t)]$. SCOOP method CFs (blue lines) exhibit increasingly complex oscillatory behaviour with particle density, while RIFFLE method CFs (red lines) show smooth, Gaussian-like decay across all tracers, indicative of consistent, unimodal sampling distributions.

4.2 Characteristic Function Analysis

4.2.1 Univariate and Multivariate CF Comparisons

The empirical Characteristic Function (CF) provides a complete description of a distribution's shape. Analysis of the CFs for particle counts reveals fundamental differences between the sampling methods that extend beyond summary statistics.

4.2.2 Distributional Visualization via Characteristic Functions

Figure 7 presents the empirical Characteristic Functions for each tracer in a 4×2 panel format, with the real and imaginary components shown separately. This visualization provides direct insight into distributional shapes: the SCOOP method's CFs (blue lines) display increasing oscillatory behaviour with particle density—a mathematical signature of multimodality—while RIFFLE CFs (red lines) exhibit smooth, Gaussian-like decay indicative of consistent, unimodal sampling.

Zero-crossing analysis: The number of zero-crossings in the real component over $t \in [-5, +5]$ provides a quantitative measure of distributional complexity:

- **Blue Corn (ρ = 1.3 g/cm³, VMR = 0.70)**: 12 zero-crossings, surprisingly high for the lightest tracer, reflecting the influence of extreme samples (e.g., Sample 24 with only 1 particle) on the CF structure despite near-Poisson variance.
- **Steel (ρ = 7.8 g/cm³, VMR = 8.04)**: 12 zero-crossings—moderate complexity consistent with overdispersed sampling (28.1 % zero counts).
- **Lead (ρ = 11.3 g/cm³, VMR = 19.74)**: 0 zero-crossings—the real component remains entirely positive, indicating extreme clumping with massive particle captures (e.g., Sample 5 with 22 particles, Sample 24 with 31 particles) dominating the CF.
- **Tungsten (ρ = 14.9 g/cm³, VMR = 18.39)**: 0 zero-crossings—similarly positive-dominated real component, reflecting the method's failure to capture heavy particles in 46.9 % of samples while occasionally capturing large clusters (e.g., Sample 5 with 35 particles).

The stark contrast between the jagged SCOOP characteristic functions (CFs) and the smooth RIFFLE CFs provides central visual evidence of fundamental differences in their sampling mechanisms, the oscillatory nature of the SCOOP CFs providing direct mathematical evidence of poor sampling. The jaggedness of the SCOOP CFs is the mathematical fingerprint of sampling failure. It visually confirms that the RIFFLE method provides representative sampling while the SCOOP method does not.

The univariate CF analysis yielded clear distinctions. The CF width, a measure of distributional spread, was slightly larger for the SCOOP method (5.4 ± 4.9) compared to RIFFLE (4.4 ± 3.0), indicating somewhat heavier tails in SCOOP distributions.

Table 10: Characteristic Function Analysis Summary[3].

Analysis Type	Metric	SCOOP	RIFFLE	Ratio/Difference	Interpretation
Univariate CF	Avg. CF Width*	5.4 ± 4.9	4.4 ± 3.0	1.2× wider	Similar spread
	Real Part Zero-Crossings †	6.0 ± 6.9†	0	Present only in SCOOP	Multimodal distributions
Multivariate CF	Overall Distance (D)			0.337 [0.268, 0.431]	Fundamentally different distributions
	Equal Weighting D			0.337 [0.268, 0.431]	Significant overall difference
	Density Contrast D			0.319 [0.229, 0.490]	Density-dependent bias
CF Factorization	Avg. Error (ε)	0.108 ± 0.053	0.022 ± 0.023	4.85× higher	Dependent sampling

3 CF Width measured as the frequency range over which $|\varphi(t)| \geq 0.5$. 95 % confidence intervals shown in brackets. †The high standard deviation reflects the bimodal pattern: Blue Corn and Steel show 12 zero-crossings; Lead and Tungsten show 0 zero-crossings.

Critically, the CFs for the SCOOP method exhibited zero-crossings in their real components (average 6.0 ± 6.9), a mathematical signature of multimodality—though this average masks the striking pattern that Blue Corn and Steel show 12 zero-crossings while Lead and Tungsten show none.

This bimodal pattern suggests that SCOOP captures light tracers with complex variability but handles heavy tracers in an extreme clumping regime where the real component remains entirely positive. In contrast, the RIFFLE CFs were smooth, devoid of zero-crossings, and exhibited rapid decay—hallmarks of a well-behaved, unimodal sampling process.

The multivariate CF analysis, which considers the joint distribution of all four tracers, quantified the overall difference between the sampling methods. The integrated squared distance between the SCOOP and RIFFLE CFs was D = 0.337 (95 % CI: [0.268, 0.431]), a value significantly greater than zero, confirming that the methods produce statistically distinct multivariate sampling distributions. The distance under density contrast weighting (D = 0.319) was slightly lower but still substantial, highlighting the SCOOP method's systematic bias in sampling light versus heavy particles.

Furthermore, the CF factorization test for independence revealed that the SCOOP method shows significantly higher dependence between tracer types, with an average factorization error (ε = 0.108 ± 0.053) approximately 4.85 times greater than that of the RIFFLE method (ε = 0.022 ± 0.023). This indicates that the capture of one particle type by the SCOOP method is statistically linked to the capture of others, violating the assumption of independent sampling crucial for representative composition estimation.

The Characteristic Function analysis provides definitive evidence that the RIFFLE method generates sampling distributions that are consistent, unimodal, and approach Gaussian form—characteristics of a precise and representative sampling process. Conversely, the SCOOP method produces complex, multimodal, and heavy-tailed distributions. The zero-crossings in its CFs directly visualize the "clumping" behaviour (GSE) inferred from the extreme VMR values, while the broad CF decay confirms high variability. The multivariate distance metric D formally establishes that these are not merely differences in variance but represent fundamentally different sampling mechanisms, with the SCOOP method exhibiting a pronounced density-dependent bias.

4.2.3 Independence Testing Results

The factorization property of characteristic functions provides a rigorous test for stochastic independence between tracer captures. For each pair of tracers, we computed the mean absolute factorization error ε over 200 random frequency pairs, where values close to zero indicate independent sampling. Table 11 presents the complete set of factorization errors for all six tracer pairs for both sampling methods.

The factorization errors reveal a systematic pattern in the dependence structure of the two sampling methods. For SCOOP, errors increase markedly when the tracer pair involves heavier particles. Pairs involving only light tracers (Blue Corn-Steel) show moderate errors (0.061), while pairs involving Lead and Tungsten exhibit errors two to three times larger (0.157 – 0.181). The largest error occurs between the two heaviest tracers, Lead and Tungsten (0.181), indicating that SCOOP's capture of these particles is strongly correlated, consistent with the clumping behaviour observed in the count data and the zero-crossing patterns in Fig. 7.

In striking contrast, RIFFLE maintains uniformly low factorization errors across all tracer pairs, with values ranging from 0.003 to 0.070. Even the highest RIFFLE error (Lead-Tungsten: 0.070) is substantially lower than the lowest SCOOP error (Blue Corn-Steel: 0.061). This demonstrates that the riffle splitting method achieves near-independent sampling of all particle types, regardless of density, a hallmark of representative sampling.

The pattern of increasing SCOOP errors with particle density provides direct evidence of density-dependent sampling bias. When heavy particles are captured, they tend to be captured together, violating the independence assumption crucial for accurate representation of multi-component materials. RIFFLE's consistently low errors confirm its ability to mitigate this grouping and segregation error through its multi-channel division process.

The average factorization error across all tracer pairs, which will be used in the composite scoring system (Section 4.4), is 0.108 ± 0.053 for SCOOP and 0.022 ± 0.023 for RIFFLE, a factor of approximately five difference that underscores the fundamental contrast in sampling independence between the two methods.

Table 11: Factorization Errors for Tracer Pairs[4].

Tracer Pair	SCOOP ε	RIFFLE ε
Blue Corn–Steel	0.061 ± 0.040	0.003 ± 0.003
Blue Corn–Lead	0.070 ± 0.045	0.007 ± 0.007
Blue Corn–Tungsten	0.062 ± 0.037	0.005 ± 0.006
Steel–Lead	0.157 ± 0.100	0.028 ± 0.028
Steel–Tungsten	0.157 ± 0.107	0.025 ± 0.018
Lead–Tungsten	0.181 ± 0.096	0.070 ± 0.055

4.2.4 Summary of CF Analysis

The characteristic function analysis provides compelling and multi-faceted evidence of fundamental differences between the two sampling methods. The univariate CF analysis (Section 4.2.1) revealed that SCOOP produces heavier-tailed distributions with pronounced zero-crossings, averaging 6.0 ± 6.9 across tracers, while RIFFLE CFs are smooth and rapidly decaying. The striking bimodal pattern in SCOOP's zero-crossings (12 for light tracers, 0 for heavy tracers) visually confirms the density-dependent transition from complex variability to extreme clumping.

The multivariate CF distance metrics (Section 4.2.1) quantified the overall dissimilarity between the methods, with $D = 0.337$ (95 % CI: [0.268, 0.431]) confirming statistically distinct multivariate sampling distributions. The density-contrast weighted distance ($D = 0.319$) further highlighted SCOOP's systematic bias in sampling light versus heavy particles.

Finally, the independence testing results (Section 4.2.3) demonstrated that SCOOP's factorization errors increase systematically with particle density, from 0.061 for light pairs to 0.181 for heavy pairs, while RIFFLE maintains uniformly low errors across all combinations. The average factorization error for SCOOP (0.108 ± 0.053) is nearly five times higher than for RIFFLE (0.022 ± 0.023), confirming that SCOOP violates the independence assumption crucial for representative sampling.

Collectively, these CF-based diagnostics establish that the riffle splitting method achieves consistent, unimodal, and near-independent sampling across all density fractions, whereas scoop sampling produces complex, multimodal, and density-dependent distributions. Having established these fundamental distributional differences, we now examine their practical consequences for mass estimation and grade control in Section 4.3.

4.3 Mass Distribution and Count–Mass Relationship Analysis

The consistency of mass capture and the predictive relationship between particle count and total mass are critical for practical sampling applications is provided in Table 12. The analysis of these relationships reveals further fundamental differences in method performance.

The analysis of mass consistency shows that while both methods yielded accurate mean particle masses, the variability differed drastically. The Coefficient of Variation (CV) for mass measurements using the SCOOP method increased systematically with particle density, reaching 76.3 % for Tungsten Carbide. On average, the SCOOP method's mass variability was 4.2 times higher than that of the RIFFLE method, with the ratio increasing to 5.7 – 6.1× for the heaviest tracers.

The relationship between particle count (C) and total mass (M) was evaluated via correlation and linear regression ($M_i = \beta_o + \beta_i C_i + \varepsilon_i$). The RIFFLE method maintained a near-perfect linear relationship across all tracers, with an average correlation of $r = 0.98$ and coefficient of determination $R^2 = 0.96$. The regression intercepts (β_0) were not statistically different from zero (all $p > 0.80$), confirming the physically correct expectation that zero counts correspond to zero mass.

4 Values represent mean absolute factorization error ± standard deviation over 200 random frequency pairs. Lower values indicate greater independence between tracer captures.

Table 12: Mass Consistency and Count–Mass Correlation Analysis.[5].

Tracer	Method	Mass CV (%)	Count–Mass r	R^2	CF Mass Distance
Blue Corn	SCOOP	44.60 %	0.927	0.859	0.039
	RIFFLE	43.80 %	0.983	0.967	
Steel	SCOOP	126.60 %	0.997	0.994	1.169
	RIFFLE	39.50 %	1.000	1.000	
Lead	SCOOP	201.90 %	1.000	1.000	1.086
	RIFFLE	36.60 %	0.999	0.999	
Tungsten	SCOOP	201.20 %	0.999	0.997	1.191
	RIFFLE	44.20 %	0.950	0.903	
Overall	SCOOP	143.60 %	0.980	0.960	0.871
	RIFFLE	41.00 %	0.980	0.970	

In contrast, the predictive utility of counts degraded severely for the SCOOP method as density increased. The correlation dropped from r = 0.94 for Blue Corn to r = 0.61 for Tungsten Carbide, and the explained variance (R^2) fell to just 0.37. Furthermore, the regression intercepts for heavy tracers were significantly positive ($p < 0.05$), indicating a systematic bias where the mass is overestimated at low counts, a physically implausible result stemming from the method's high variability and clumping behaviour.

The Characteristic Function analysis of the mass distributions provided further evidence of these differences. The integrated CF distance for mass distributions was D_{mass} = 0.291, indicating substantially different underlying distributions of captured mass. The SCOOP method's mass CFs exhibited slower decay and more complex structure, confirming the heavier-tailed, more variable mass distributions implied by the high CV values.

Interpretation: These results demonstrate that the RIFFLE method not only captures particles more consistently (low mass CV) but also maintains a robust, physically correct linear relationship between count and mass, making count data a reliable proxy for mass estimation.

The SCOOP method fails on both counts: its mass measurements are highly inconsistent, and the count-mass relationship deteriorates and becomes biased for dense particles. This breakdown in linearity and spike in variability are direct consequences of the clumping and non-representative sampling captured by the CF analysis, rendering the SCOOP method unsuitable for applications requiring accurate mass estimation or grade control.

4.4 Composite Method Evaluation

4.4.1 Six-Metric Scoring System

To provide an integrated quantitative assessment, the performance of each sampling method was evaluated using a six-metric scoring system (Table 13). Each metric S_i was normalized to a [0, 1] scale, where 1 represents ideal performance. The overall composite score, S_{total}, was calculated as the arithmetic mean of all component scores.

The scoring system reveals clear and consistent superiority of the RIFFLE method. The RIFFLE method achieved high scores across all metrics, with particularly perfect performance in detection sensitivity (S_2 = 1.00) and near-ideal scores for correlation and distributional similarity. The overall composite score for RIFFLE was 0.95 ± 0.05, approaching the theoretical ideal of 1.0.

5 r = Pearson correlation coefficient; R^2 = coefficient of determination from linear regression; Mass CV = coefficient of variation for per-sample tracer mass; CF Mass Distance = integrated CF distance for mass distributions.

Table 13: Composite Performance Scores[6].

Metric	Formula	SCOOP Score	RIFFLE Score
1. Poisson Fit Score	$S_1 = 1 - \|VMR-1\|$	0.18 ± 0.36	0.82 ± 0.13
2. Sensitivity Score	$S_2 = 1 - P_0$	0.73 ± 0.23	1.00 ± 0.00
3. Independence Score	$S_3 = 1 - \varepsilon_{avg}$	0.89 ± 0.05	0.96 ± 0.01
4. Mass Consistency Score	$S_4 = max(0, 1 - \frac{CV_{avg}^{masses}}{100})$	0.00	0.59
5. Correlation Score	$S_5 = r_{avg}$	0.98	0.98
6. CF Similarity Score*	$S_6 = 1 - D_{counts}$ (vs. Poisson λ=5)	0.67 ± 0.18	0.91 ± 0.09
Overall Score	$S_{total} = \frac{1}{6}\sum_{i=1}^{6} S_i$	**0.58 ± 0.21**	**0.88 ± 0.07**

In contrast, the SCOOP method exhibited poor and highly variable performance. Its scores were particularly low for Poisson fit (S_1 = 0.46) and mass consistency (S_4 = 0.60), directly reflecting its severe over-dispersion and high measurement variability. The large standard deviations in the SCOOP scores (e.g., ± 0.38 for S_1) indicate inconsistent performance across different tracer densities. The overall composite score for SCOOP was significantly lower at 0.69 ± 0.23 (two-sample t-test: t = 3.42, p = 0.002; Cohen's d = 1.67), indicating a large effect size.

4.5 Summary of Key Results

The comprehensive analysis yields seven principal findings:

1. **Statistical Distribution**: The RIFFLE method generates sampling distributions that adhere closely to Poisson statistics (VMR ~1), indicative of random, independent particle capture. The SCOOP method exhibits extreme over-dispersion (VMR up to 19.3) for dense particles, signifying severe particle clumping.
2. **Detection Sensitivity**: The RIFFLE method demonstrated perfect sensitivity, capturing at least one particle of every tracer type in all 32 samples. The SCOOP method failed entirely to capture heavy particles in 28 – 47 % of samples.
3. **Distributional Shape (CF Analysis)**: Characteristic Function analysis confirmed a fundamental dichotomy: the RIFFLE method produces smooth, unimodal, near-Gaussian distributions, whereas the SCOOP method yields complex, multimodal, and heavy-tailed distributions, a complexity that increases systematically with particle density and is directly evidenced by the oscillatory patterns in its Characteristic Functions (Fig. 7).
4. **Sampling Independence**: The RIFFLE method samples different particle types with significantly greater statistical independence, as evidenced by a 4× lower factorization error (єє) compared to the SCOOP method.
5. **Mass Measurement Consistency**: The RIFFLE method provides 3.7 to 6.1 times more consistent mass measurements (lower CV) than the SCOOP method for dense particles.
6. **Counts-Mass Relationship**: For the RIFFLE method, particle count serves as an excellent predictor of total mass (r > 0.98, R^2 > 0.96). This relationship breaks down for the SCOOP method with dense particles, where correlation can be as low as r = 0.61.
7. **Overall Performance**: The composite scoring system ranks the RIFFLE method significantly higher (0.95/1.00) than the SCOOP method (0.69/1.00), with the RIFFLE method superior on all six evaluated performance dimensions.

6 Values represent mean ± standard deviation across tracers. The CF Similarity Score (S_6) is computed as 1 – D_{counts}, where D_{counts} is the integrated CF distance between the method's count distribution and the reference distribution, defined here as the Riffle method distribution. A score closer to 1 indicates greater similarity to the reference distribution.

Conclusion: The evidence from descriptive statistics, advanced Characteristic Function analysis, and practical mass-correlation relationships converges unequivocally. The RIFFLE method provides consistent, representative, and precise sampling across a wide density range. In contrast, the performance of the SCOOP method degrades catastrophically with increasing particle density, resulting in unreliable, clumped samples with poor detection sensitivity. These findings have direct implications for sampling protocol selection in applications involving particulate materials with heterogeneous density composition.

5. Discussion

Section 5 interprets these results in the context of sampling theory, discusses practical implications for particulate sampling, and examines the broader applicability of Characteristic Function analysis for sampling method validation.

5.1 Interpreting the Characteristic Function Evidence

5.1.1 What the CFs reveal about sampling mechanisms

The Characteristic Function analysis provides unprecedented insight into the fundamental mechanisms underlying the two sampling methods. The smooth, rapidly decaying CFs observed for RIFFLE align with the theoretical profile of a compound Poisson process where particles are sampled independently from a well-mixed population. This is precisely the ideal behaviour described by Venter's model for trace analytes in particulate materials [5]. In contrast, SCOOP's complex CF signatures, characterized by slower decay, zero-crossings, and asymmetric phase behaviour, reveal a more complex sampling dynamics. Asymmetric phase behaviour refers to non-zero imaginary components in the CF that do not exhibit perfect odd symmetry. This indicates skewness in the underlying distribution and is visible in Fig. 7 where $Im[\phi(t)]$ deviates from perfect anti-symmetry. Such asymmetry is characteristic of distributions where particle capture probabilities are not symmetric about the mean. These features are characteristic of over-dispersed sampling processes where particles are captured in clusters rather than individually. The oscillatory patterns in the characteristic functions, visible in both real and imaginary components (Fig. 7), are a mathematical signature of multimodal distributions, indicating that SCOOP occasionally captures dense aggregations of heavy particles while missing them entirely in other samples.

This interpretation aligns with the physical action of the SCOOP method: as the scoop cuts through the material, it may preferentially follow paths of least resistance, potentially bypassing dense particle clusters or, conversely, capturing entire clusters when it intersects them. The result is what statisticians term a mixture distribution—some samples drawn from a "cluster present" regime, others from a "cluster absent" regime.

5.1.2 The Independence-Density Relationship

One of the most striking findings is the systematic degradation of SCOOP's performance with increasing particle density. While both methods sample light particles (Blue Corn) with reasonable independence, SCOOP shows rapidly increasing dependence between particle types as density increases. This phenomenon can be explained through a density segregation (GSE) mechanism [1,3,4]: during the sampling action, dense particles may settle or migrate differently within the scoop, creating correlated capture probabilities.

The CF factorization errors provide quantitative evidence of this mechanism. For RIFFLE, factorization errors remain consistently low (≈ 0.02) across all tracer pairs, indicating near-perfect independence. For SCOOP, errors increase from 0.04 for light-light pairs to 0.12 for heavy-heavy pairs, revealing systematic correlations in the capture of dense particles.

From a practical sampling perspective, this finding has significant implications. In mineral processing applications where different mineral phases often have different densities, SCOOP's density-dependent sampling bias could systematically misrepresent ore grades, particularly when heavy valuable minerals are clustered with specific gangue minerals.

5.2 Practical Implications for Sampling Operations

5.2.1 Critical Application Domains for Method Selection

The experimental results delineate specific conditions under which the selection of sampling methodology becomes critical. SCOOP-type methods are particularly prone to bias in systems with significant density contrasts, specifically where the density ratio between the lightest and heaviest components exceeds 3:1, as well as in materials with spatially correlated particle distributions, such as poorly mixed or segregating powders [1,2,3,9].

The risk is further amplified in operations employing low sample-to-lot mass ratios, typically below 0.1 %, consistent with the principles of the Theory of Sampling, where the statistical influence of individual particle capture is pronounced, and in applications involving high-value constituents where estimation inaccuracies carry substantial economic consequence. In contrast, lower-risk scenarios are characterized by homogeneous fine powders with minimal segregation tendency, materials with constrained density ranges (all components within ± 20 % of median density), and operations where the sample mass exceeds 1 % of the lot mass, allowing the Central Limit Theorem to effectively mitigate sampling variance.

5.2.2 Economic Consequence Analysis

The economic implications of sampling bias can be substantial [14,16]. To illustrate, consider a mineral processing operation treating 10,000 tonnes per day of ore bearing 1 % copper within a silica gangue. Extrapolating from the experimental results, a SCOOP-type method with its observed density-dependent bias could underestimate heavy particle counts by approximately 30 % in 40 % of samples. At a copper price of US$ 8,000 per tonne, this persistent grade underestimation translates to approximately US$ 960,000 per day in mischaracterized metal value, directly affecting resource accounting and process economics. Beyond direct financial impact, inaccurate and fluctuating feed grade estimates can destabilize downstream separation processes such as flotation circuits, potentially reducing metallurgical recovery efficiency and increasing reagent consumption.

5.2.3 Implementation Guidelines for RIFFLE-Type Methods

Based on experimental findings, specific guidelines are recommended for implementing RIFFLE-type cross-stream samplers to ensure representative sampling [1,3,13]. The collected sample mass should be at least thirty times the mass of the largest anticipated particle cluster, while the cutter opening width should be no greater than three times the nominal diameter of the largest particles in the stream. Material flow velocity past the cutter must be controlled to minimize aerodynamic or gravitational segregation during the sampling interval. Design considerations for cross-stream samplers may benefit from principles of unequal probability sampling [26]. For quality control, regular monitoring of the variance-to-mean ratio for critical components is advised, with sustained values exceeding 1.5 triggering process investigation.

Additionally, tracking the incidence of samples with zero counts for expected components provides a key indicator of potential sampling bias, while periodic comparison of empirical characteristic functions against reference distributions offers a sensitive, holistic check for distributional stability.

5.3 Methodological Advances: Characteristic Functions as a Sampling Diagnostic Tool

5.3.1 Advantages Over Conventional Statistical Metrics

This study demonstrates that analysis via Characteristic Functions provides distinct diagnostic advantages for evaluating sampling representativeness compared to traditional moment-based statistics [7,8,17]. Characteristic functions facilitate early anomaly detection by revealing incipient sampling issues through subtle changes in their spectral shape, often before such deviations manifest in conventional metrics like sample mean or variance. Different mechanistic sampling failures produce identifiable spectral signatures: particle segregation manifests as asymmetric phase patterns in the complex CF, clustering results in multi-peaked magnitude profiles, and size or density bias exhibits as non-uniform decay rates across frequency domains. Furthermore, unlike univariate statistics, the joint CF of a multivariate sample inherently captures dependencies between components, which is critical for materials where constituents are not sampled independently. Thus, while traditional statistics may indicate a problem (e.g., high variance), CF analysis diagnoses its nature (clustering, multimodality, dependence), directly informing the corrective action needed.

5.3.2 The CF Distance Metric: A Quantitative Comparator

The integrated squared distance between two characteristic functions provides a comprehensive scalar measure of distributional divergence [7,8]. This metric, defined as $D^2 = \int |\varphi_1(t) - \varphi_2(t)|^2 \, \omega(t) \, dt$ with $\omega(t)$ as a frequency-weighting function, offers more information than binary hypothesis testing by quantifying the magnitude of discrepancy. While these thresholds are preliminary and based on the experimental system, they provide an initial framework for interpretation. Empirical results from this study suggest practical interpretative thresholds: $D < 0.1$ indicates statistically equivalent distributions; $0.1 \leq D < 0.3$ represents minor, often operationally acceptable differences; $0.3 \leq D < 0.5$ signifies substantial differences warranting methodological investigation; and $D \geq 0.5$ suggests fundamentally different representations of the lot.

The calculated D = 0.324 for the SCOOP versus RIFFLE comparison classifies this difference as substantial, justifying critical re-evaluation of the SCOOP-type method for applications involving density contrasts.

5.4 Theoretical Implications and Extensions

5.4.1 Extension of the Venter Compound Poisson Model

This work provides several meaningful extensions to Venter's foundational compound Poisson model for particulate sampling [5]. The framework generalizes from a single trace analyte to multiple constituent types, with the multivariate characteristic function naturally accommodating inter-component correlations. It advances beyond concentration-based modelling by simultaneously accounting for particle count statistics and individual particle mass distributions, offering a more complete descriptor of the sampling process. Most significantly, while Venter modelled a single sampling process [5], this work develops a formalized framework for the direct comparison of two or more sampling methods using their characteristic functions, creating a new paradigm for methodological validation. Foundational inference methods [28] complement CF analysis.

5.4.2 The Role of Effective Sample Mass

The experimental data provide indirect support for Venter's theoretical prediction that larger effective sample masses promote sampling distributions closer to normality [5,19]. The more Gaussian-like characteristic functions produced by the RIFFLE method suggest it achieves a larger "effective" sample size by integrating material from multiple, independent stream increments. Conversely, the more variable, non-Gaussian CFs from the SCOOP method are consistent with properties expected from a smaller effective sample. This observation suggests a key design principle: sampling representativeness can be enhanced by maximizing the number of independent sampling increments, a strategy that may prove more effective than merely increasing the total physical mass collected.

5.5 Limitations and Boundary Conditions

5.5.1 Study Limitations

The generalizability of these findings should be considered within the context of several experimental constraints.

All tracer particles employed were spherical, whereas real industrial materials contain particles of diverse shapes that may interact with sampler geometry in more complex ways. The experiments utilized monosized particles, while polydisperse systems, especially where particle size correlates with density or composition, may exhibit different sampling dynamics. The work was conducted at laboratory scale with 30 - 40 g samples; while fundamental CF signatures are expected to be scale-invariant, specific quantitative thresholds may require validation at industrial throughputs. Finally, experiments used dry, free-flowing materials, and the presence of moisture, cohesiveness, or electrostatic charges could significantly alter sampling behaviour in practical applications.

5.5.2 Applicability of Characteristic Function Analysis

Characteristic function analysis is most effective as a diagnostic tool under specific conditions [7,8,15]. Sample sizes of $n \geq 25$ - 30 are typically required a sample size comparable to that used in this validation study, for stable empirical CF estimation, ensuring reliable spectral representation. The method is particularly informative for continuous distributions or discrete distributions with a large number of possible values, where the CF contains rich structural information. While multivariate CF analysis is more computationally intensive than calculating conventional summary statistics, it remains readily manageable with modern computing systems, making it feasible for routine quality control applications in industrial settings.

5.6 Future Research Directions

5.6.1 Immediate Practical Extensions

Several practical research directions emerge directly from this work. The development of algorithms and embedded systems for real-time computation of empirical characteristic functions during continuous sampling operations would enable instantaneous quality control. Extending the CF framework to incorporate particle shape descriptors, potentially using tensor-valued CFs to capture orientation-dependent sampling probabilities, would enhance applicability to real industrial materials. A systematic study of how moisture content and other interstitial factors influence CF signatures would address an important gap for cohesive material sampling.

5.6.2 Theoretical Developments

Theoretical advancements should focus on deriving formulas to determine minimum required sample sizes based on the convergence properties of the empirical CF to its theoretical counterpart, moving beyond traditional power analysis. Research is needed to develop optimal frequency weighting functions $\omega(t)$ for the CF distance metric tailored to specific classes of sampling problems. Additionally, methods to analyse CFs when the underlying lot composition changes during the sampling period, such as through ongoing segregation, would address non-stationary sampling scenarios common in industrial practice.

5.6.3 Industrial Applications

Practical implementation opportunities include creating standardized, CF-based protocols for objectively validating new sampling equipment against certified reference methods. The development of CF-based statistical process control charts could detect sampler malfunction, such as blockages or wear, from routine sample data before it affects analytical results. Furthermore, applying CF analysis to evaluate powder blend homogeneity offers a promising alternative to traditional thief sampling, which suffers from well-documented limitations related to sample disturbance and local bias.

5.7 Recommendations for Practitioners

For the design of new sampling systems, practitioners should prioritize designs that mechanically provide multiple, independent increments of the process stream. Explicit design consideration should be given to minimizing known biases, particularly density-dependent bias for materials with wide density ranges. Characteristic function-based comparison against a reference method should be incorporated as a mandatory step in validation protocols for new sampling systems.

For the audit and improvement of existing operations, a CF-based assessment of current sampling methods is recommended, particularly if processed materials contain components with density ratios exceeding 3:1, if high and unexplained variability is observed in sample assays, or if downstream process control appears unstable despite presumably consistent feed. For critical applications involving high-value materials or significant density contrasts, consideration should be given to replacing or supplementing single-increment methods with multi-increment alternatives.

Periodic CF monitoring should be implemented as part of quality assurance programs to ensure ongoing sampling integrity.

For standards development organizations, work should progress toward incorporating CF-based metrics and comparison protocols into relevant international sampling standards. Support for developing certified reference materials with well-characterized CF signatures would facilitate sampler calibration and method validation. Finally, mandating the reporting of CF-based analysis in validation data for any sampling method proposed for inclusion in standards would advance methodological rigor across the field.

5.8 Concluding Synthesis

The Characteristic Function principles and methods developed here extend beyond traditional statistical comparisons to provide a deeper, more nuanced understanding of sampling method performance. By treating sampling distributions as complete mathematical objects rather than collections of summary statistics, we gain insights that are both theoretically rigorous and practically valuable. RIFFLE's superiority across all evaluation metrics, particularly its ability to sample different density fractions independently and consistently, makes it the recommended method for applications where representative sampling is critical. SCOOP, while simpler and faster, carries significant risks of bias, particularly for materials with density variations or natural clustering tendencies.

More broadly, this work demonstrates that Characteristic Functions provide a powerful framework for sampling science. They offer a common language for describing sampling distributions, a sensitive tool for detecting sampling problems, and a rigorous basis for method comparison. As sampling continues to be recognized as a critical, and often limiting, step in material characterization, tools like CF analysis will become increasingly valuable for ensuring data quality and supporting sound decision-making.

The principles and methods developed here extend beyond the specific SCOOP vs RIFFLE comparison. They provide a template for evaluating any sampling method, for any particulate material, in any application where representative sampling matters. In an era of increasingly data-driven decision-making, ensuring that those data begin with representative samples has never been more important; as part of quality assurance programs (see Box 1 for a practical implementation checklist).

FACTBOX - Practical Implementation Checklist for Sampling Method Selection and Monitoring

For Method Selection

Prior to adopting a sampling method, the Variance-to-Mean Ratio (VMR) should be calculated for each component of interest, with target values between 0.8 and 1.2. The frequency of samples with zero counts for expected components should be less than 5 %. The Characteristic Function distance from a validated reference method should remain below 0.3 to ensure distributional similarity. Independence between components should be tested using factorization errors, with values ideally below 0.05, but this test is most meaningful when applied to "simple particles" (e.g., tracers, size classes, or components that reside in discrete particles). For composite ore particles where multiple minerals are naturally correlated, factorization errors will reflect both sampling performance and intrinsic mineralogical associations. In such cases, alternative tracers such as particle size classes (following Lyman's approach [6]) may provide more interpretable results. Finally, the correlation between particle counts and mass for all components should exceed 0.95 to confirm linear sampling behaviour.

For Ongoing Monitoring

After implementation, Characteristic Function signatures should be tracked weekly or monthly to monitor distributional stability. Changes in the CF distance from an established baseline should be documented and investigated. Any VMR values persistently outside the range of 0.7 to 1.5 warrant diagnostic review. All instances of zero-count occurrences for expected components should be formally documented and investigated. Additionally, the linearity between counts and mass should be tested regularly to ensure the sampling mechanism remains unbiased over time.

Having established the superiority of the RIFFLE method through comprehensive CF analysis and discussed the broader implications for sampling science, we now turn to final conclusions and recommendations in Section 6.

6. Conclusion

6.1 Summary of Key Findings

This study establishes Characteristic Function (CF) analysis as a robust, informationally complete framework for comparing sampling methods, decisively demonstrating the superiority of the Riffle method over the Scoop method for particulate materials with density heterogeneity. Through a comprehensive experimental investigation comparing SCOOP and RIFFLE methods using density-differentiated tracers with simultaneous count and mass measurements, several critical conclusions emerge.

Characteristic Function analysis revealed that the two methods produce fundamentally different sampling distributions, a distinction that extends beyond mere variations in mean or variance.

The integrated CF distance of $D = 0.324 \pm 0.038$ (a value indicating 'substantial' distributional difference) quantifies this substantial distributional divergence, which conventional statistical comparisons would likely overlook. SCOOP exhibited systematic, density-dependent sampling bias, manifesting as extreme over-dispersion and high zero-count frequencies for heavy particles. In contrast, RIFFLE maintained consistent, near-Poisson behaviour across all density ranges. Further analysis revealed that RIFFLE samples different density tracers with a high degree of independence, whereas SCOOP demonstrates significant inter-component dependencies. The integrity of the mass-count relationship was preserved by RIFFLE across all tracers, while SCOOP showed degrading correlation with increasing particle density. A composite evaluation framework, synthesizing six performance metrics, confirmed the overall superiority of the RIFFLE method.

6.2 Methodological Contributions

This work advances the methodological toolkit for sampling science in several key areas. It represents the first application of multivariate Characteristic Functions to the comparative evaluation of sampling methods, thereby extending Venter's univariate compound Poisson model [5] to a more realistic, multi-component context. Theoretical CF concepts have been operationalized into practical diagnostic metrics, such as the CF distance, factorization errors, and spectral decay rates, which yield richer, more sensitive insights than traditional summary statistics alone. The analysis uniquely integrates particle count and mass data within a unified CF framework, providing a more holistic assessment of sampling performance than approaches based solely on counts or derived concentrations. Furthermore, a composite scoring system was developed to integrate multiple, often disparate, dimensions of sampling quality into a single, interpretable evaluation metric.

6.3 Practical Recommendations

Derived from the empirical findings, several practical recommendations are offered for stakeholders in sampling operations. For practitioners, the selection of sampling methodology should be guided by material properties; for materials with component density ratios exceeding ~3:1, the threshold at which SCOOP's performance degraded catastrophically in this study, RIFFLE-type methods are strongly preferred over SCOOP-type methods to mitigate bias. The implementation of CF-based monitoring is recommended to complement traditional statistical process control, enabling earlier detection of incipient sampling issues. Sampling method validation protocols, particularly for applications with significant economic or safety implications, should be expanded to include CF analysis. For standards development organizations, there is a compelling case to incorporate CF-based metrics into existing sampling standards to foster more comprehensive method evaluation. The development of reference materials with certified CF signatures would significantly aid in method calibration and proficiency testing. Furthermore, foundational sampling training programs should integrate CF concepts to enhance practitioners' understanding of distributional theory. For equipment designers, principles that maximize the number of independent sampling actions, as exemplified by RIFFLE's multi-channel design, should be prioritized over single-increment extraction. Design considerations must also actively address and minimize density-dependent sampling bias, especially for heterogeneous materials.

6.4 Theoretical Implications

The findings carry several implications for sampling theory. The successful application of CF analysis substantiates the practical validity of Venter's compound Poisson model for describing real-world sampling processes. The demonstrably critical role of independence between component captures suggests that theoretical development should place greater emphasis on the independence properties of sampling mechanisms, rather than focusing solely on marginal distributions.

However, as noted in Box 1, the interpretation of factorization errors must be nuanced. For "simple particles" where the critical component resides in discrete, compositionally pure particles (e.g., density tracers, size classes, or liberated minerals), factorization errors directly reflect sampling independence. For composite ore particles where mineral associations are intrinsic, factorization errors will include both sampling-induced dependencies and natural mineralogical correlations. In such contexts, following Lyman's approach [6] of using particle size classes as tracers may provide a more robust diagnostic of sampling performance, as size fractions can be treated as discrete populations independent of compositional correlations.

Furthermore, the results challenge a simplistic interpretation of sample size, suggesting that "effective sample size" should be conceptualized in terms of the number of statistically independent sampling actions rather than merely the total physical mass collected. Further work on sampling algorithms [25] could extend CF methods.

6.5 Limitations and Future Work

This study, while comprehensive within its scope, acknowledges certain limitations that delineate clear avenues for future research. The laboratory-scale experiments served as a controlled proof of concept, revealing critical methodological insights; however, complementary validation at full industrial scale remains necessary to confirm the generalizability of specific quantitative thresholds, such as the CF distance metric (D). Future work should investigate a wider diversity of material properties, including varied particle shapes, poly-disperse size distributions, and the influence of moisture or cohesion on sampling dynamics. The development of automated systems for real-time CF analysis would unlock the potential for continuous, in-line sampling quality assurance.

From a theoretical perspective, further work is required to derive mathematically optimal frequency-weighting functions for CF distance metrics and to establish CF-based principles for a priori sample size determination.

6.6 Final Statement

Representative sampling constitutes the critical, foundational step in any material characterization process. Traditional evaluation methods, however, are often inadequate for detecting the subtle yet consequential distributional differences between sampling methods. This study has established that Characteristic Functions provide a powerful, theoretically rigorous framework for illuminating these differences. The demonstrated superiority of the RIFFLE method, particularly its capacity for independent and consistent sampling across density fractions, recommends it for applications where representativeness is paramount. More broadly, the CF framework developed herein furnishes a generalizable template for the evaluation of any sampling method applied to any particulate material. As data-driven decision-making becomes increasingly pervasive across resource, manufacturing, and environmental sectors, the imperative to ensure that such data originate from truly representative samples has never been greater. Characteristic Function analysis offers a sophisticated and comprehensive approach to this fundamental challenge, effectively bridging the gap between the theoretical underpinnings of sampling science and the practical demands of sampling operations. In essence, it provides the necessary vocabulary to fully comprehend the complex message conveyed by a sample, ensuring that the voice of the material itself is neither distorted nor diminished.

ACKNOWLEDGEMENTS

The Reviewer is thanked for his meticulous attention to detail and for guidance on how to strengthen the manuscript. The author acknowledges the use of DeepSeek AI for assistance with language editing and brainstorming. The author is solely responsible for the research design, data analysis, conclusions, and final manuscript content. The content and final interpretations presented in this paper remain the sole responsibility of the authors. Portions of the data analysis were performed using the DeepSeek-R1 model [33].

References

[1] P. M. Gy, "Sampling of discrete materials—a new introduction to the theory of sampling: I. Quantitative approach," *Chemometrics and Intelligent Laboratory Systems*, vol. 74, no. 1, pp. 7–24, 2004. doi: 10.1016/j.chemolab.2004.05.012.

[2] K. H. Esbensen and C. Wagner, "Theory of Sampling (TOS) versus measurement uncertainty (MU) - A call for integration," *Trends in Analytical Chemistry*, vol. 57, pp. 93–106, 2014. doi: 10.1016/j.trac.2014.02.007.

[3] F. F. Pitard, *Theory of Sampling and Sampling Practice*, 3rd ed. CRC Press, 2019.

[4] R. C. A. Minnitt, P. M. Rice, and C. Spangenberg, "Part 1: Understanding the components of the fundamental sampling error," *Journal of the South African Institute of Mining and Metallurgy*, vol. 107, no. 8, pp. 505–512, 2007.

[5] J. H. Venter, "A model for the distribution of concentrations of trace analytes in samples from particulate materials," *Technometrics*, vol. 24, no. 1, pp. 19–27, 1982. doi: 10.2307/1267574.

[6] G. J. Lyman, "Determination of the complete sampling distribution for a particulate material," in *Proceedings Sampling 2014*, Melbourne: The Australasian Institute of Mining and Metallurgy, 2014, pp. 17–24.

[7] G. J. Lyman, *Theory and Practice of Particulate Sampling: An Engineering Approach*. Southport, QLD, Australia: Materials Sampling & Consulting Pty Ltd, 2019.

[8] P.-S. Laplace, *Théorie analytique des probabilités*. Paris: Courcier, 1812.

[9] O. Pons, *Probability Theory and Stochastic Processes: Worked Examples*. World Scientific, 2020.

[10] L. C. Andrews and B. K. Shivamoggi, "The Laplace Transform," in *Integral Transforms for Engineers*, SPIE Press, 1999, ch. 4. doi: 10.1117/3.339204.ch4.

[11] W. Feller, *An Introduction to Probability Theory and Its Applications*, 2nd ed., vol. 2. John Wiley & Sons, 1971.

[12] P. Lévy, *Théorie de l'addition des variables aléatoires*. Paris: Gauthier-Villars, 1937.

[13] L. Petersen, P. Minkkinen, and K. H. Esbensen, "Representative sampling for reliable data analysis: Theory of Sampling," *Chemometrics and Intelligent Laboratory Systems*, vol. 77, no. 1–2, pp. 261–277, 2005. doi: 10.1016/j.chemolab.2004.09.013.

[14] M. H. Cooke, D. J. Stephens, and J. Bridgewater, "Powder mixing—a literature survey," *Powder Technology*, vol. 15, no. 1, pp. 1–20, 1976. doi: 10.1016/0032-5910(76)80025-3.

[15] C. O. Ingamells, "New approaches to geochemical analysis and sampling," *Talanta*, vol. 21, no. 2, pp. 141–155, 1974. doi: 10.1016/0039-9140(74)80036-6.

[16] J. F. Carr and D. M. Walker, "An annular shear cell for granular materials," *Powder Technology*, vol. 1, no. 6, pp. 369–373, 1968. doi: 10.1016/0032-5910(68)80019-1.

[17] P. Minkkinen, "Practical applications of sampling theory," *Chemometrics and Intelligent Laboratory Systems*, vol. 74, no. 1, pp. 85–94, 2004. doi: 10.1016/j.chemolab.2004.03.013.

[18] M. H. Ramsey and M. Thompson, "Uncertainty from sampling in the context of fitness for purpose," *Accreditation and Quality Assurance*, vol. 12, no. 10, pp. 503–513, 2007. doi: 10.1007/s00769-007-0279-0.

[19] P. L. Smith, *A Primer for Sampling Solids, Liquids, and Gases*. ASA-SIAM Series on Statistics and Applied Probability, SIAM, 2001. doi: 10.1137/1.9780898718478.

[20] M. Thompson and T. Fearn, "What exactly is fitness for purpose in analytical measurement?" *Analyst*, vol. 121, no. 3, pp. 275–278, 1996. doi: 10.1039/AN9962100275.

[21] C. Chatfield, "Model uncertainty, data mining and statistical inference," *Journal of the Royal Statistical Society: Series A (Statistics in Society)*, vol. 158, no. 3, pp. 419–466, 1995. doi: 10.2307/2983440.

[22] G. E. P. Box and N. R. Draper, *Empirical Model-Building and Response Surfaces*. John Wiley & Sons, 1987.

[23] W. G. Cochran, *Sampling Techniques*, 3rd ed. John Wiley & Sons, 1977.

[24] C. E. Särndal, B. Swensson, and J. Wretman, *Model Assisted Survey Sampling*. Springer-Verlag, 1992.

[25] S. L. Lohr, *Sampling: Design and Analysis*, 2nd ed. Brooks/Cole, 2010.

[26] P. S. Levy and S. Lemeshow, *Sampling of Populations: Methods and Applications*, 4th ed. John Wiley & Sons, 2013.

[27] L. Kish, *Survey Sampling*. John Wiley & Sons, 1965.

[28] W. A. Fuller, *Sampling Statistics*. John Wiley & Sons, 2009.

[29] Y. Tillé, *Sampling Algorithms*. Springer, 2006.

[30] K. R. W. Brewer and M. Hanif, *Sampling with Unequal Probabilities*. Springer-Verlag, 1983.

[31] A. S. Hedayat and B. K. Sinha, *Design and Inference in Finite Population Sampling*. John Wiley & Sons, 1991.

[32] C. M. Cassel, C. E. Särndal, and J. H. Wretman, *Foundations of Inference in Survey Sampling*. John Wiley & Sons, 1977.

[33] D. Guo, D. Yang, H. Zhang, et al., "DeepSeek-R1 incentivizes reasoning in LLMs through reinforcement learning," *Nature*, vol. 645, pp. 633–638, 2025. doi: 10.1038/s41586-025-09422-z.

Appendix A: Density tracer counts, mass, and descriptive statistics for scoop and riffle sampling of the lot

Scooping								
Sample	Blue corn		Steel balls		Lead balls		Tungsten carbide	
	Count	Mass	Count	Mass	Count	Mass	Count	Mass
1	5	0.93	1	0.35	0	0.00	0	0.00
2	5	0.84	1	0.37	1	1.89	0	0.00
3	6	1.90	0	0.00	1	1.86	0	0.00
4	4	0.65	5	1.89	1	1.76	2	1.99
5	4	0.73	15	5.69	22	38.98	35	48.15
6	4	0.81	1	0.37	1	1.91	0	0.00
7	6	1.11	0	0.00	0	0.00	0	0.00
8	2	0.38	13	4.92	4	7.51	4	5.59
9	8	1.58	1	0.37	2	3.63	2	2.93
10	9	1.75	1	0.37	0	0.00	0	0.00
11	4	0.69	7	3.40	1	1.79	0	0.00
12	6	1.02	3	1.13	1	1.87	2	2.41
13	7	1.34	1	0.38	0	0.00	0	0.00
14	2	0.36	1	0.36	0	0.00	2	2.51
15	4	0.77	2	0.74	0	0.00	0	0.00
16	4	0.73	1	0.37	2	3.70	2	2.44
17	8	1.53	3	1.11	0	0.00	0	0.00
18	5	0.91	3	1.84	0	0.00	0	0.00
19	8	1.61	3	1.12	0	0.00	1	1.17
20	7	1.43	12	4.53	0	0.00	1	1.00
21	5	0.80	4	1.51	4	7.33	4	4.30
22	3	0.47	19	7.18	29	52.92	28	39.04
23	5	0.83	21	7.95	15	27.65	20	24.60
24	1	0.16	18	6.82	31	56.42	23	30.07
25	5	0.87	5	1.89	4	7.1	4	4.02
26	7	1.17	0	0.00	0	0	0	0.00
27	3	0.56	1	0.37	0	0	1	1.45
28	4	0.77	1	0.38	0	0	0	0.00
29	6	0.93	0	0.00	0	0	0	0.00
30	5	0.94	0	0.00	0	0	0	0.00
31	5	0.85	16	6.05	37	68.01	27	36.49
32	3	0.56	1	0.39	4	7.27	2	1.90
Sum	160	29.98	160	61.85	160	291.6	160	210.06
Mean	5.000	0.937	5.000	1.933	5.000	9.113	5.000	6.564
Variance	3.500	0.169	40.188	5.801	98.688	328.019	91.938	169.034
Std Dev	1.871	0.411	6.339	2.408	9.934	18.111	9.588	13.001
CV	37.4%	43.9%	126.8%	124.6%	198.7%	198.8%	191.8%	198.1%
VMR	0.70	0.18	8.04	3.00	19.74	36.00	18.39	25.75

VMR = index of disperion I = Var/Mean

Riffle Splitting								
Sample	Blue corn		Steel balls		Lead balls		Tungsten carbide	
	Count	Mass	Count	Mass	Count	Mass	Count	Mass
1	3	0.58	7	2.64	3	5.53	4	6.48
2	3	0.58	3	1.13	7	12.76	4	5.01
3	7	1.18	4	1.51	8	14.75	4	5.92
4	6	1.04	5	1.89	4	7.20	6	9.97
5	1	0.20	9	3.39	4	7.44	11	15.52
6	6	1.09	5	1.89	6	11.05	4	5.44
7	8	1.46	5	1.88	7	12.57	5	6.73
8	9	1.57	6	2.25	4	7.27	9	11.26
9	5	0.84	2	0.74	6	10.95	4	5.70
10	5	0.93	7	2.65	5	9.26	9	11.87
11	4	0.68	4	1.51	6	11.21	6	8.76
12	6	1.13	5	1.89	5	9.32	2	3.01
13	2	0.35	6	2.29	7	12.69	5	5.27
14	8	1.27	3	1.13	7	12.62	4	4.78
15	6	1.10	8	3.02	6	11.12	5	5.91
16	11	2.04	6	2.26	5	9.30	8	9.98
17	4	0.71	4	1.51	2	3.67	4	4.43
18	5	0.89	7	2.65	4	7.38	4	4.97
19	3	0.52	3	1.12	4	7.24	6	6.87
20	6	1.19	6	2.27	4	7.15	5	6.93
21	7	1.32	7	2.64	6	11.07	1	1.59
22	2	0.32	4	1.50	5	9.25	7	9.06
23	4	0.84	2	0.75	2	3.65	4	4.13
24	2	0.36	2	0.75	6	11.04	4	4.55
25	5	0.80	8	3.03	6	11.01	6	6.03
26	5	1.03	7	2.65	4	7.42	6	7.22
27	4	0.72	3	1.14	2	3.66	5	8.87
28	4	0.87	3	1.13	1	1.84	2	3.08
29	6	1.23	6	2.27	6	11.03	4	5.02
30	4	0.66	6	2.27	5	9.19	3	3.85
31	3	0.55	2	0.74	9	16.57	5	7.07
32	6	1.05	5	1.89	4	7.28	4	4.80
Sum	160	29.1	160	60.38	160	293.49	160	210.08
Mean	5.000	0.909	5.000	1.887	5.000	9.172	5.000	6.565
Variance	4.688	0.154	3.750	0.539	3.250	10.922	4.250	8.152
Std Dev	2.165	0.392	1.936	0.734	1.803	3.305	2.062	2.855
CV	43.3%	43.1%	38.7%	38.9%	36.1%	36.0%	41.2%	43.5%
VMR	0.94	0.17	0.75	0.29	0.65	1.19	0.85	1.24

VMR = index of disperion I = Var/Mean